Uncovering flow instabilities and the role of inter-particle surface friction in shear-thickening suspensions of colloidal rods

This dissertation is submitted for the degree of
M.S.(Engg.)

by

Mohit Chaudhary

Chemistry and Physics of Materials Unit
Jawaharlal Nehru Centre for Advanced Scientific Research
Bangalore - 560 064

SEPTEMBER, 2021

To my parents and sisters

DECLARATION

I hereby declared that the matter embodied in the thesis entitle "**Uncovering flow instabilities and the role of inter-particle surface friction in shear-thickening suspensions of colloidal rods**" is a result of investigations carried out by me at the Chemistry and Physics of Materials Unit, Jawaharlal Nehru Centre for Advanced Scientific Research, Bangalore, India under the supervision of Prof. Rajesh Ganapathy and that it has not been submitted elsewhere for the award of any degree or diploma. In keeping with the general practice in reporting scientific observations, due acknowledgments has been made wherever the work described is based on the findings of other investigators.

Mohit Chaudhary

CERTIFICATE

I hereby certify that the matter embodied in this thesis entitled "**Uncovering flow instabilities and the role of inter-particle surface friction in shear-thickening suspensions of colloidal rods**" has been carried out by Mr. Mohit Chaudhary at the Chemistry and Physics of Materials UNit, Jawaharlal Nehru Centre for Advanced Scientific Research, Bangalore, India under my supervision and that it has not been submitted elsewhere for the award of any degree or diploma.

Prof. Rajesh Ganapathy
(Research Supervisor)

Acknoweldgements

First of all, I want to thank my supervisor Prof. Rajesh Ganapathy, to whom I owe the deepest gratitude for his constant support, guidance, and motivation throughout the academic and non-academic work. The work which I have done would not be possible without his help and advice. Working with him has been a thoroughly enjoyable experience, and his contagious enthusiasm for science has motivated me at various times. His valuable comments and instructions in writing this thesis have helped me immensely. I am incredibly grateful for his kindness, endless support, and encouragement.

I am very grateful to all the Soft Matter Lab past and present group members: Pragya, Niloy, Navneet, Manodeep, Divya, Uttam, Subhanshi, and Srimoyee, who helped me in many ways while carrying out my research work, and during thesis writing. I am grateful to all the wonderful people I met in JNC, specially Raagya, Ashish, Sabarish, Akshay, Amit, Ekashmi, Aditi, Anjana, Chitrang, and Ruchika, who have made my journey in JNC memorable and cherishing. I am highly indebted to all my course instructors Prof. Ganesh Subramanian, Prof Srikanth Sastry, Prof. Subir K Das, and Prof Balasubramanian. Their classes during the coursework immensely helped me in my research. Being friendly to the students always, it's been a great pleasure to discuss any scientific and non-scientific issues with them. I convey the most profound respect to those teachers in my school and college who always inspired and motivated me to pursue higher studies.

Finally, it will be an incomplete task if I forget to acknowledge all my family members. It's their unconditional love and support which helped me accomplish my dream.

Synopsis

Shear thickening (ST) is a well-known phenomenon observed in suspensions, characterized by an increase in viscosity with applied shear stress. Recent advancement in our understanding indicates the role of inter-particle surface contact friction in ST of dense suspensions. In such suspensions with an increase in volume fraction of particles, ST also increases and transits from continuous shear thickening (CST) to discontinuous shear thickening(DST). In the DST regime, the presence of a negative slope in shear-stress versus shear-rate plot indicates the presence of flow instability. No such instability is expected or observed in the CST regime. In this thesis, we study whether surface friction of the particles plays any role in ST, and are flow instabilities present in suspensions of anisotropic particles in the CST regime.

This thesis consists of four chapters. Chapter 1 provides a brief introduction to two different models which try to explain ST in suspensions. The first model is the hydrodynamic model and the second one is the inter-particle frictional model. In the latter part of this chapter, various strategies for tuning ST are discussed. Chapter 2 provides details of the experimental setup and synthesis protocols followed to synthesize silica colloidal rods and coat them with temperature-sensitive polymers. Chapter 3 discusses the findings from our studies which can be subdivided into two different sections. In the first section, temperature-sensitive polymer-coated colloidal rods are used to tune the surface friction and their flow behavior as a function of temperature is studied by suspending them in aqueous medium. In the second section, flow instabilities are explored in the CST regime in the suspensions of silica colloidal rods and water-glycerol mixture.

To do so, stress relaxation measurements are performed at different volume fractions for two different measuring system geometries. Chapter 4 concludes our findings and provides insight into our understanding of the subject so far.

List of Figures

Contents

Chapter 1

INTRODUCTION

1.1 Fluids

Fluids are defined as materials that are unable to withstand shearing forces and undergo a continuous and unrecoverable change once sheared [1]. All fluids in response to an externally applied shear force provide resistance to flow, which is quantified by a term called viscosity (η), defined as proportionality constant in Newton's law of viscosity (equation 1.1).

$$\sigma = \eta\dot{\gamma} \tag{1.1}$$

where σ is the shear-stress and $\dot{\gamma}$ is the shear-rate which is defined as the first time derivative of shear-strain. Based on the above definition, fluids can be classified into two different categories:

1. **Newtonian fluids**
   These are the fluids in which the viscosity remains constant with applied shear-stress or shear-rate and is represented as green curve in Figure 1.1. Examples are water, alcohol, hexane, etc.

2. **Non-Newtonian fluids**
   These are the fluids that show deviation from Newton's law of viscosity. Viscosity of such fluids changes as a function of σ or $\dot{\gamma}$. If η decreases with σ, we call such fluids as shear thinning, and if η increases with σ, we call them shear thickening fluids as represented in Figure 1.1 by the yellow and red curves respectively. Examples of shear thinning fluids are toothpaste, blood, quicksand, etc., whereas, for shear thickening, we have oobleck, slurries, silly-putty, etc.

The general behavior of such fluids can be captured by the modified form of Newton's
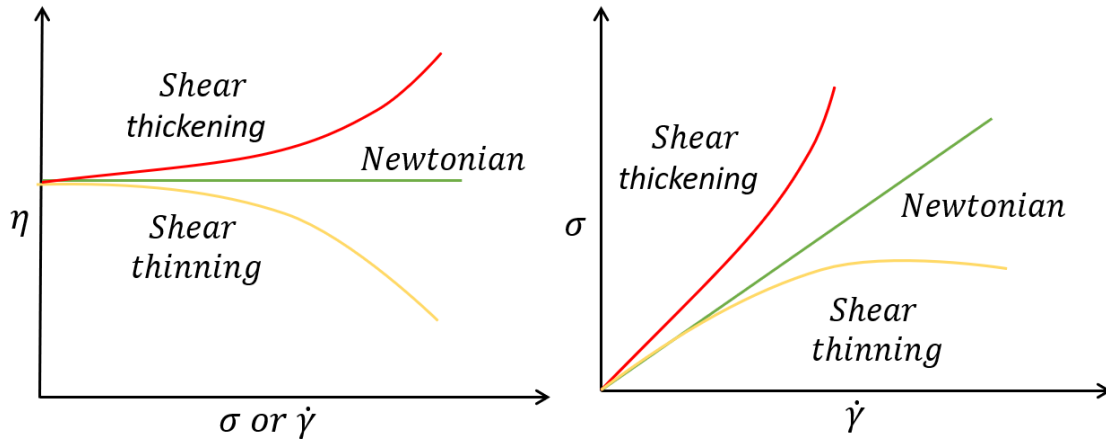
Figure 1.1: Flow behavior of different types of fluids. Green curve corresponds to Newtonian fluid while the yellow and red curves corresponds to non-Newtonian behavior called shear thinning and shear shear thickening fluids respectively.

law of viscosity also called Herschel-Bulkley model defined as

$$\sigma = \sigma_\circ + k\left(\frac{dv}{dy}\right)^n \tag{1.2}$$

where

'$\sigma_\circ$' - yield stress;

'k' - flow consistency index;

'n' - flow behavior index;

'dv/dy' - velocity gradient.

In this model, for shear thickening fluids $k > 0$ and $n > 1$, and for shear thinning fluids $k > 0$ and $0 < n < 1$. For $n = 1$ and $\sigma_\circ=0$, equation 1.1 is recovered with $k = \eta$. This model is good for describing flow in materials such as fresh concrete, mud suspension, lava, etc. [3, 4, 5].

1.2   Suspensions

A suspension is a heterogeneous mixture of solid particles suspended freely in a continuous fluid medium. Common examples include cornstarch and water mixture, paint, milk, blood, etc. The stability of such suspensions depends on their ability to counter aggregation and phase separation, which depends on parameters such as inter-particle
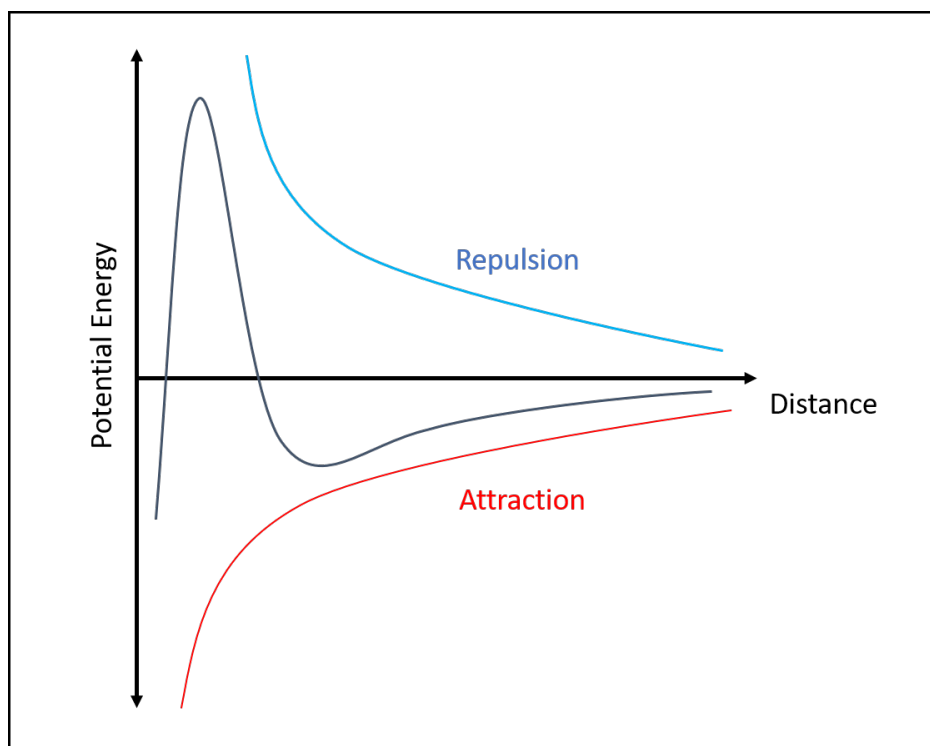
Figure 1.2: Potential around a particle with distance resulting from electrostatic stabilization method. The blue curve corresponds to the repulsive interaction due to the presence of an electric double layer, the red curve corresponds to van der Waals interaction between the particles, and the black curve corresponds to effective potential felt by the particles.

interactions, the magnitude of Brownian and gravitation forces on particles. If particles interact via attractive dispersion forces such as van der Waals interactions, the suspension is more likely to be unstable [6, 7, 8]. Experimentally, the stability of such suspensions is ensured by two methods.

- **Steric stabilization**: This mechanism involves adsorption of large molecules or polymeric chains on the surface of the particles. This coating creates a repulsive force ensuring finite surface separation [9, 10, 11].

- **Electrostatic stabilization**: In this method repulsive Coulomb forces are utilized to counterbalance attractive van der Waals forces [12, 13]. The presence of surface charge on the particle leads to an electric double layer formation: Stern layer and diffusive layer [14]. Potential in the double layer is maximum on the particle's surface and reduces to zero at the boundary of the double layer. The resulting potential is the total contribution due to van der Waals and electrostatic

potential terms and can be expressed as:

$$V_{total} = V_{vw} + V_e$$
$$V_{total} = -\frac{Ar}{12x} + 2\pi\varepsilon\varepsilon_\circ\varsigma^2 e^{-kx} \tag{1.3}$$

where

'r' - radius of the particle;

'A' - Hamaker constant;

'x' - distance from the surface;

'ς' - zeta potential;

'k' - Debye-Huckel parameter.

The resulting effective potential term is represented in Figure 1.2 by the grey curve which depends on Debye length given by k^{-1}. With increase in ionic concentration, particle surface becomes more shielded resulting in decreased Debye length.

1.2.1   Dilute suspensions

For a fluid consisting of particles suspended in the dilute limit, flow profile remains closely Newtonian with η higher than that of the fluid alone. For dilute suspensions, total viscosity can be written as the sum of two different contributions: $\eta_\circ$ and $\eta\prime$, where $\eta_\circ$ is the suspending medium viscosity, and $\eta\prime$ is the contribution to viscosity due to suspended particles. For spherical particles, η can be expressed as

$$\eta = \eta_\circ(1 + \frac{5}{2}\phi) \tag{1.4}$$

where ϕ is the particle volume fraction [15]. For a spheroidal particle with semi-axes as a and $b = c$, resulting viscosity can be expressed as

$$\eta = \eta_\circ(1 + A\phi) \tag{1.5}$$

where values of A are written in table 1.1 [16].

a/b	0.1	0.2	0.5	1.0	2	5	10
A	8.04	4.71	2.85	2.5	2.91	5.81	13.6

Table 1.1: Values of A for a spheroidal particle suspensions of different aspect ratios.

Equation 1.4 is known as the Einstein relation. It holds well when $\phi < 0.02$ [17],

but severely underestimates the viscosity at higher ϕ because of the inter-particle interactions contribution to η. By taking Brownian diffusion and hydrodynamic interactions into account, Batchelor extended Einstein's work further and derived

$$\eta = \eta_\circ(1 + 2.5\phi + K\phi^2) \tag{1.6}$$

where $K = 6.2$ [18]. The above relation holds well for ϕ below 0.15-0.20 [19].
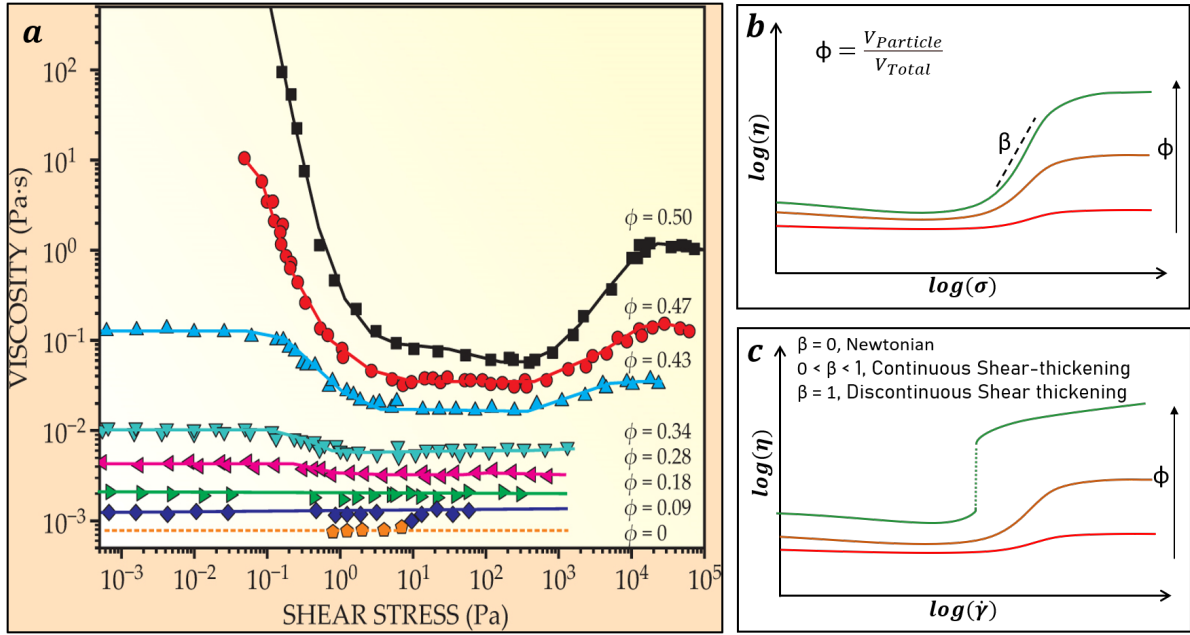
Figure 1.3: General behavior observed in concentrated suspensions. (a) η vs σ plot for colloidal latex dispersion for different ϕ. At lower values of ϕ, viscosity is almost constant. While at higher ϕ, shear thinning and shear thickening can be observed. Reproduced from [20], with the permission of the American Institute of Physics. (b) and (c) are schematics to understand role of β in quantifying the extent of shear thickening and to differentiate between continuous shear thickening and discontinuous shear thickening.

1.2.2   Concentrated suspensions

At higher values of ϕ, η displays non-monotonic behavior as a function of both σ and $\dot{\gamma}$ in suspensions(Figure 1.3 (a)). Many-body interactions, lubrication forces, and inter-particle contact forces come into play, and suspension viscosity no more remains a constant. All forms of non-Newtonian behaviors such as yield stress, shear thinning, shear thickening can be observed in the same sample. At lower stresses, one needs to overcome yield stress to generate flow in the sample which is followed by the first Newtonian plateau. Shear thinning is observed on further increasing σ followed by

the second Newtonian plateau, also called high-shear Newtonian plateau. At higher stresses, suspension starts shear thickening (ST) until η saturates to a constant value depending on ϕ. With ϕ, the increase and decrease in η with σ in the shear thickening and the shear thinning stress window becomes more prominent and highly depends on the inter-particle interactions and the shape of particles. For example, shear thickening occurs at lower volume fractions in suspensions of anisotropic particles such as rods and ellipsoids than in isotropic particles such as spheres. It is because anisotropic particles tend to have more excluded volume and higher solvent deflection around the particles [21, 22, 23].

The extent of shear thickening is quantified by an exponent β, also shown in Figure 1.3 (b), which is zero for Newtonian fluids, $0 < \beta < 1$ during continuous shear thickening (CST) (red and brown curve in Figure 1.3 (c)) and $\beta \geq 1$ during discontinuous shear thickening (DST) (green curve in Figure 1.3 (c)). For most of the stable particulate suspensions, the transition from CST to DST is achieved by increasing ϕ. On further increasing ϕ, suspension shear jams and stable flow is not expected.
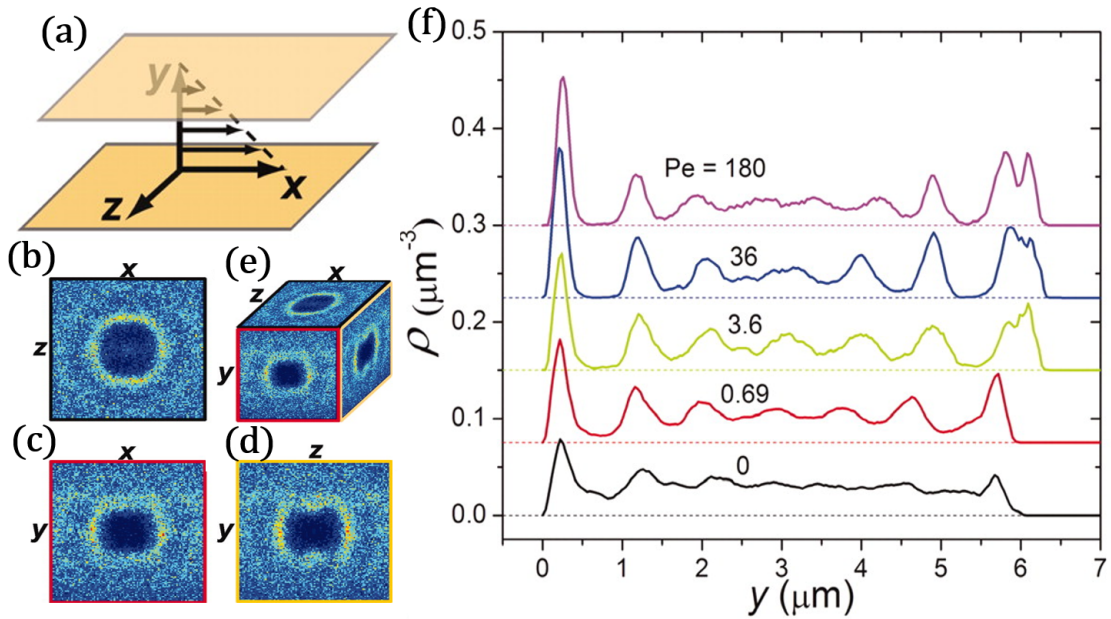
Figure 1.4: (a) Reference coordinate system. (b-e) g(r) for a sample containing monodispersed spherical silica particles of diameter $0.96\mu m$ in water-glycerin mixture at $\phi = 0.34$ and $Pe = 0.036$. (b-d) shows $g(r)$ in xz, xy and zy planes. (f) Plot of particle density along flow gradient direction for different Pe. All panels are from [24]. Reprinted with permission from AAAS.

1.3 Shear thinning in concentrated suspensions

The shear thinning regime in concentrated suspensions is observed at lower values of σ and is caused by a flow induced transition from an entropically favored state to an ordered state. This behavior is observed when the $\dot{\gamma} > (\tau_\alpha)^{-1}$, where τ_α is the relaxation time, defined as the time taken by particle to move its own diameter. For $\dot{\gamma} < (\tau_\alpha)^{-1}$, flow is sufficiently slow to counter relaxation of the microstructures to entropically favored configuration. Light scattering experiments on suspensions have indicated that shear thinning transition is related to rearrangements of particles into layers, which decreases the total dissipation of energy under shear. For monodispersed particles, such experiments revealed the formation of hexagonally packed layered-like structures [25, 26]. Single-particle resolution fast confocal microscopy also fetched out similar results [24] as shown in Figure 1.4 (f), which clearly points towards the presence of periodic narrow dense regions along the y-axis. The pair-correlation function $g(r)$ plotted with respect to reference coordinate system shown in Figure 1.4 (a), displays anisotropy in the plane having normal along the vorticity (xy plane) and velocity direction (yz plane) (Figure 1.4 (b)-(d)). Higher intensity of the horizontal bands in $g(x,y)$ and $g(y,z)$ plots indicates increased layering, thereby reducing η by lowering dissipation through inter-particle collisions [27, 28].

Stokesian dynamics simulations yielded similar results for spherical particles under shear [29]. Detailed structural analysis of the layers indicated a weak stringy configuration of particles for moderate values of ϕ and distorted hexatic for ϕ close to bulk crystallization density for hard spheres.

1.4 Shear thickening in concentrated suspensions

Shear thickening in dense suspensions can be observed at higher stresses. In a flow curve, this regime happens to be adjacent to the second Newtonian plateau. A good example of such a fluid is Oobleck, a concentrated mixture of cornstarch and water roughly in 2-to-1 by volume, on which people can run across with ease only to sink when they stop. Although most of the applications depict entertainment, the study of such fluids is of great importance to enhance the efficiency of industrial processes, a significant example being the clogging of slurry pipelines during hydraulic transportation [30]. Such fluids also find wide range of potential applications in absorbing shocks and vibrations [31, 32].

As shown in Figure 1.3 (a), concentrated suspensions have a finite yield stress and shear thin on increasing σ similar to solids. But unlike solids, concentrated suspensions display an abrupt or discontinuous rise in η above a threshold σ. Even though this rise in

η in suspensions is observed to depend on parameters which can be controlled with ease experimentally, the mechanism resulting in ST behavior of suspensions as a function of these parameters remains unclear. As of now, two different theories try to explain the underlying mechanism of shear thickening through entirely different approaches. The first theory considers many-body hydrodynamic interactions, while the second theory adopts ideas from granular flow and applies it to concentrated suspensions. Both the theories are discussed in the following subsections.

1.4.1 Hydrodynamic model of shear thickening

For a single spherical particle undergoing Brownian motion, diffusion is given by

$$D_\circ = \frac{kT}{6\pi\eta a} \tag{1.7}$$

Hence on an average particle takes $a^2/D_\circ$ to diffuse distance equal to its radius. For a suspension this time scale is important because it sets a time scale for low and high shear-rate. Relevant dimensionless number which relates $\dot{\gamma}$ to thermal diffusion of the particle is called Peclet number and can be written as

$$Pe = \frac{\dot{\gamma}a^2}{D_\circ} = \frac{\sigma a^3}{kT} \tag{1.8}$$

Shear thickening is observed for $Pe > 10$ when shear dominates particle diffusion. The presence of one particle creates displacement in a liquid, which other particles can experience. This leads to fluid mediated many-particle interactions which alters the Brownian motion. Such fluid mediated interactions are called hydrodynamic interactions. In atomic or molecular fluids these interactions do not exist since intervening medium is vacuum. Hence on ignoring particle hydrodynamic coupling, viscosity should remain unchanged even when $Pe \to \infty$. For higher values of Pe, particles tend to come close to each other, and lubrication dynamics couple the particles. Since lubrication force (F_L) diverges as r^{-1}, the particle surfaces do not touch each other and because of the time reversibility of the Navier-Stokes equation, the force needed to separate the particles apart is the same as the force required to bring them together. Hence, if such a system is kept undisturbed, the particles will stay in close configuration.

For a single particle in shear-flow, test particle traces two different trajectories: trajectories extending to infinity and closed circuits (Figure 1.5 (a)) [33]. So if another particle comes in close vicinity, they orbit each other indefinitely. For a semi-dilute or a concentrated system, similar dynamics lead to the formation of large particle

clusters called hydroclusters, which are stabilized by the shear field (Figure 1.5 (c)). Such densely packed regions of particles result in higher energy dissipation, resulting in increase in η.
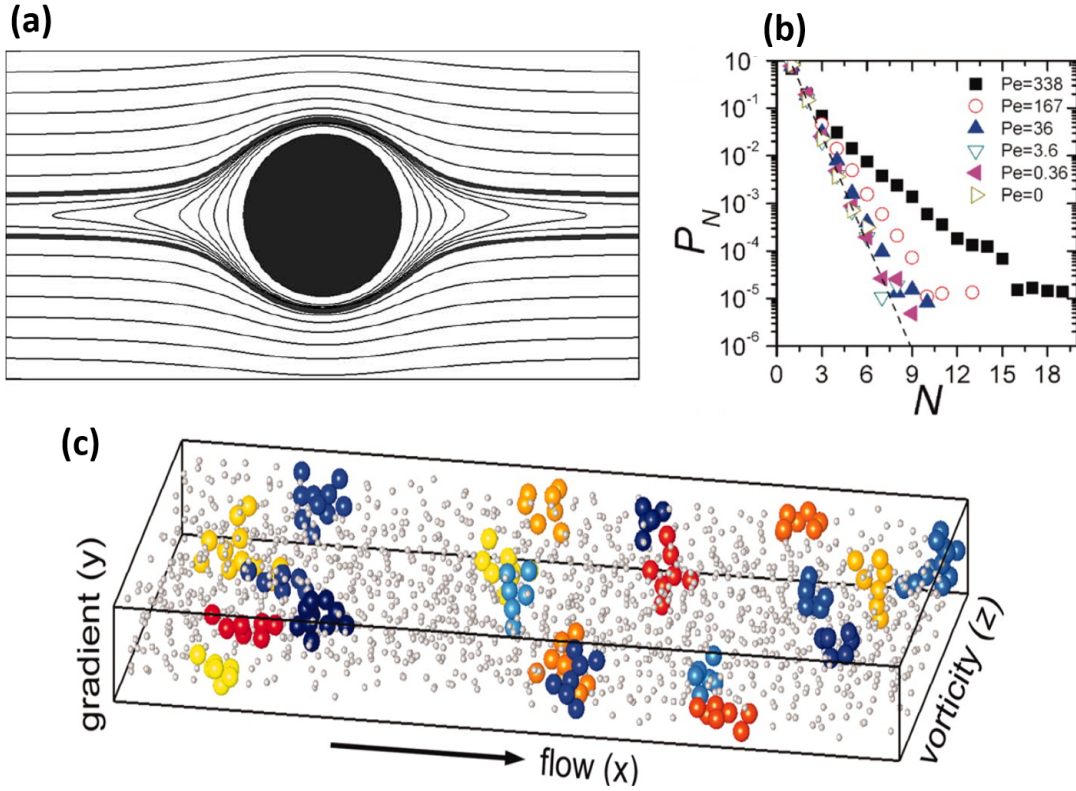
Figure 1.5: (a) Streamlines around a spherical particle in a simple shear flow in particle frame of reference. Reprinted with permission from [34].Copyright 2008, The Society of Rheology. (b) Probability distribution of clusters having N number of particles at different Pe. (c) Real time image of hydroclusters in a suspension under shear. Different hydroclusters are marked with different colours. (b) and (c) are adopted from [24]. Reprinted with permission from AAAS.

As σ is increased, the probability of finding clusters with larger number of particles also increases (Figure 1.5 (b)). As particle cluster size grows with Pe, the viscosity of the suspension also increases. But this phenomenon only gives rise to CST [35]. Stokesian dynamic simulation performed by taking only hydrodynamic interactions into account results in severe underestimation of η in concentrated regime [36, 37]. Hence this model provide no insight of the transition from CST to DST in suspensions with ϕ. The issue which is largely unconsidered in the simulations are the inter-particle contacts. All particles have some extent of surface roughness by which they can come in contact despite there being a lubrication force, thereby changing the expected response of the suspensions. Lowering of threshold $\dot{\gamma}$ and CST to DST transition at a lower ϕ is

observed in suspensions when particle surfaces are made more rough [38] and inter-particle contacts are taken into account.

1.4.2 Granular and suspension rheology

This model explains the divergence in viscosity in a suspension containing spherical particles by adopting concepts from the granular flow. Pressure-induced shear flow for granular particles and suspensions is depicted in Figure 1.6 (a). Unlike solid confining walls in granular particle apparatus, for suspension apparatus, walls are porous such that only the suspending medium is allowed to pass through (Figure 1.6 (b)). On imposing $\dot{\gamma}$ at some constant confining pressure 'P_p', such that if 'F_N' is the normal force and 'A' is the area of plate, $P_p = F_N/A$, the medium under confinement is free to compact or dilate (Figure 1.6 (c)). For such a system, dimensionless control parameter is defined as a ratio of internal time of rearrangement $t_{micro} = \eta_f/P_p$, where η_f is the suspending medium viscosity, and time of strain $t_{macro} = 1/\dot{\gamma}$, also called the viscous number

$$I_\nu = \frac{\eta_f \dot{\gamma}}{P_p} \tag{1.9}$$

and the friction coefficient μ and volume fraction ϕ becomes a simple function of I_ν.

$$\sigma = \mu(I_\nu)P_p \,, \; \phi = \phi(I_\nu) \tag{1.10}$$

When $I_\nu \to 0$, $\mu \sim 0.3$ (μ_1) which is same for particles in dry medium (granular system) or viscous medium (Figure 1.6 (d)). Depending on the value of P_p and $\dot{\gamma}$, the suspension either expands or compresses until the force balance between P_p and particle pressure is achieved. On increasing P_p, the yield stress also increases. It is mainly because increase in externally applied confinement force will lead to more fluid getting squeezed out of the plates, thereby increasing ϕ.

As $\dot{\gamma} \to 0$ or $P_p \to \infty$, I_ν approaches zero and ϕ approaches its maximum value ϕ_m=0.585 (Figure 1.6 (d)). Close to ϕ_m, behavior of ϕ can expressed $(\phi_m - \phi) \propto I_\nu^{0.5}$, which differs from the behavior observed in granular matter ie. $(\phi_m - \phi) \propto I$, where I is the inertial number [40]. When a suspension is sheared at constant ϕ, one can always write $\sigma \propto \eta_f \dot{\gamma}$ or

$$\sigma = \eta_s(\phi)\eta_f \dot{\gamma} \tag{1.11}$$

where η_s is a dimensionless effective shear-viscosity proportionality constant. Similarly
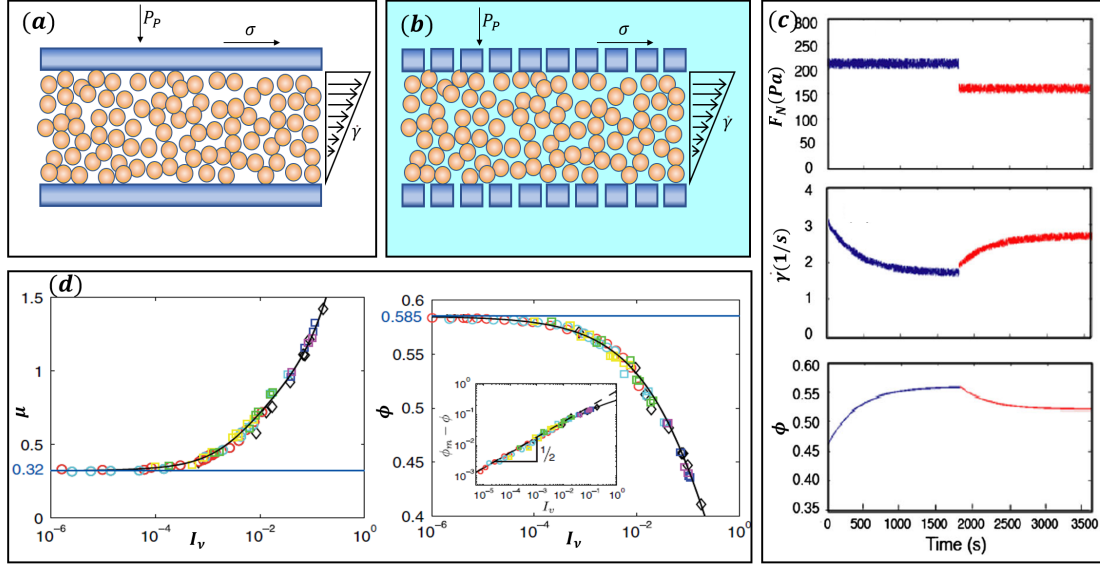
Figure 1.6: (a) and (b) are basic diagram of pressure imposed shear-flow cell for a granular suspension with dry and wet medium respectively. Plates are porous for suspension allowing only fluid to exchange. (c) for $\sigma = 150pa$, response of $\dot{\gamma}$ and ϕ with time in response to change in F_N, where F_N is P_p times the surface area. (d) Friction coefficient and volume fraction as a function of viscous number [1.1mm PMMA spheres ($\circ$), 0.58mm PS spheres ($\square$) at $\phi_\circ = 0.565$, and for PS spheres at $\phi_\circ = 0.433$ ($\diamond$), where $\phi_\circ$ is the initially loaded volume fraction]. (c)-(d) adopted from [39] with permission.

for P_p one can write similar relation as

$$P_p = \eta_n(\phi)\eta_f\dot{\gamma} \tag{1.12}$$

Where η_n is again an effective dimensionless normal-viscosity constant. Rearranging equation 1.9 and plugging the value of P_p in equation 1.10, one can easily obtain

$$P_p = \frac{1}{I_\nu}\eta_f\dot{\gamma} \; ; \; \sigma = \frac{\mu(I_\nu)}{I_\nu}\eta_f\dot{\gamma} \tag{1.13}$$

Comparing equation 1.13 to 1.11 and 1.12, one can easily identify η_s and η_n as

$$\eta_s = \frac{\mu(I_\nu)}{I_\nu} \; ; \; \eta_n = \frac{1}{I_\nu} \tag{1.14}$$

Since η_f is fixed, and $\mu \to 0.32$ as I_ν approaches zero, equation 1.14 implies both η_s and η_n should diverge when $\phi \to \phi_m$, and is found to diverge as $(\phi_m - \phi)^{-2}$.

Application of pressure imposed shear flow fixes both ϕ and σ/P_p as a function of I_ν and predicts divergence in viscosity only at ϕ_m. Hence for a fixed value of ϕ, relation be-

tween σ and $\dot{\gamma}$ is linear. As ϕ_m is approached from below, inter-particle contacts rapidly increases, leading to a divergence in $\eta(\phi)$. Above ϕ_m homogeneous flow is not possible, and one expects to see fractures or shear banding with particle migration [41, 42]. On the contrary, flow curve measurements performed on concentrated suspensions under fixed geometrical confinement and at constant ϕ display ST, while constant confining pressure experiments display quasi-Newtonian behavior for a given ϕ. It indicates that ST in concentrated suspensions is related to an increase in confining pressure, which largely depends on inter-particle repulsion.

1.4.3   Wyart and Cates model of shear thickening

In the hydrodynamic model of ST, lubrication film between the particles mediates the overall interaction. Inter-particle surfaces never come in contact with each other since F_L diverges as the surface separation approaches zero. In such a scenario, particles can always smoothly slide past each other, and the viscosity should only diverge as ϕ approaches the maximum random closed packing volume fraction, which for spherical particles is $\phi = 0.64$ (ϕ_s). But this is rarely the case and it is often observed that η diverges for $\phi < \phi_s$.
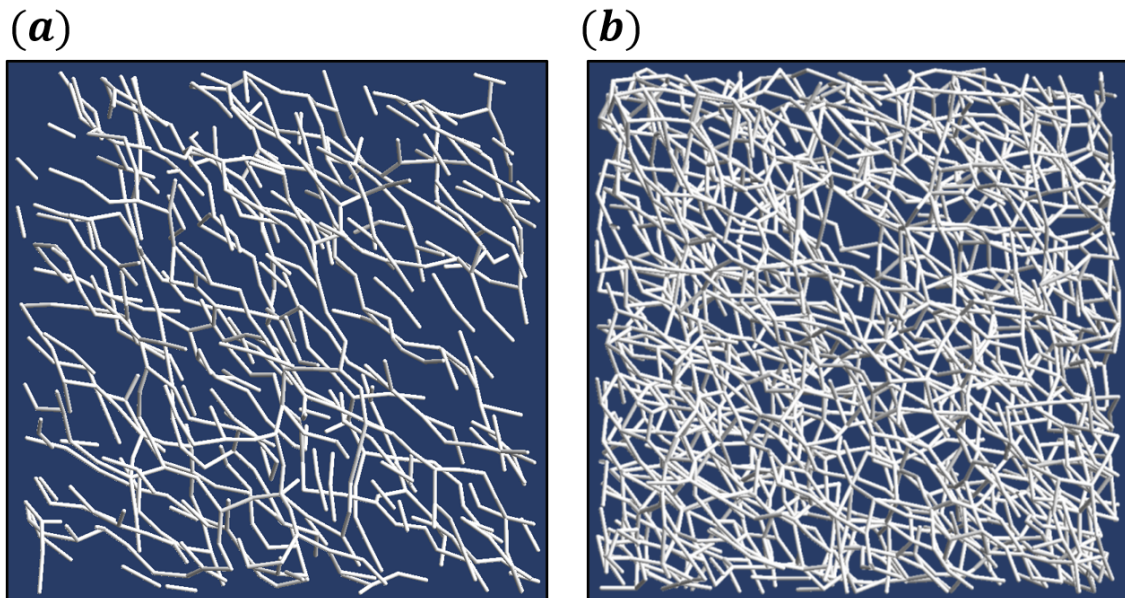
Figure 1.7: (a)-(b) Results from simulations representing frictional contacts as white bonds corresponding to $\dot{\gamma}$=0.05 (low viscosity state) and $\dot{\gamma}$=0.1 (high viscosity state). Adopted from [35] with permission.

Constant confinement pressure experiments described in the previous section indicate that for a fixed value of ϕ, ST is not observed. Instead, suspension behaves like

a quasi-Newtonian liquid with viscosity diverging as $(\phi_j - \phi)^{-2}$, where ϕ_j is jamming volume fraction. The value of ϕ_j depends on the particle surface interactions, and its value is lower for suspensions in which interactions are dominated by frictional contacts. The absence of ST under such restrictive circumstances points out the importance of confining pressure in observing this behavior. At the microscopic scale, keeping the confining pressure fixed also means imposing an upper bound on maximum normal force that two particles can experience to bring them together. In most of the rheological experiments performed on ST suspensions, the confinement is kept constant instead of P_p. For concentrated suspensions in such a scenario, P_p increase with σ. Now, if a stress scale (σ^*) is defined above which the lubrication film ruptures and particle surfaces come in contact, we transit from a quasi-Newtonian curve corresponding to a suspension in which particles can slide past each other to the one in which particles can only role and form force chain networks (Figure 1.7) Mathematically if we define σ^* such that

$$\sigma << \sigma^* : \text{mostly frictionless contacts}$$
$$\sigma >> \sigma^* : \text{mostly frictional contacts}$$

(1.15)

We can define a function '$f(\tilde{\sigma})$', where f represents the fraction of frictional contacts and $\tilde{\sigma} = \sigma/\sigma^*$, such that

$$f(\tilde{\sigma}) = 0 \text{ when } \tilde{\sigma} = 0$$
$$f(\tilde{\sigma}) = 1 \text{ when } \tilde{\sigma} \to \infty$$

(1.16)

So now we have a possibility of having both lubricated and frictional contacts between particles in a suspension depending on the value of σ. For such a system ϕ_j will also change and with increase in σ will move from $\phi_j = \phi_s \to \phi_j = \phi_m$, where ϕ_m is the jamming volume fraction when all particles interacts via frictional contacts. This smooth transition in ϕ_j can be expressed as

$$\phi_j = \phi_m f(\tilde{\sigma}) + \phi_s(1 - f(\tilde{\sigma}))$$

(1.17)

For updated value of ϕ_j, relation between σ and $\dot{\gamma}$ can now be expressed as

$$\sigma = \frac{\lambda}{(\phi_j - \phi)^2} . \dot{\gamma}$$

(1.18)

where λ is a constant with dimensions of viscosity.
To obtain DST at $\phi < \phi_m$, $1 - f(\tilde{\sigma}) < O(\tilde{\sigma}^{-1/2})$. For the choice of $f = 1 - e^{-\tilde{\sigma}}$, flow
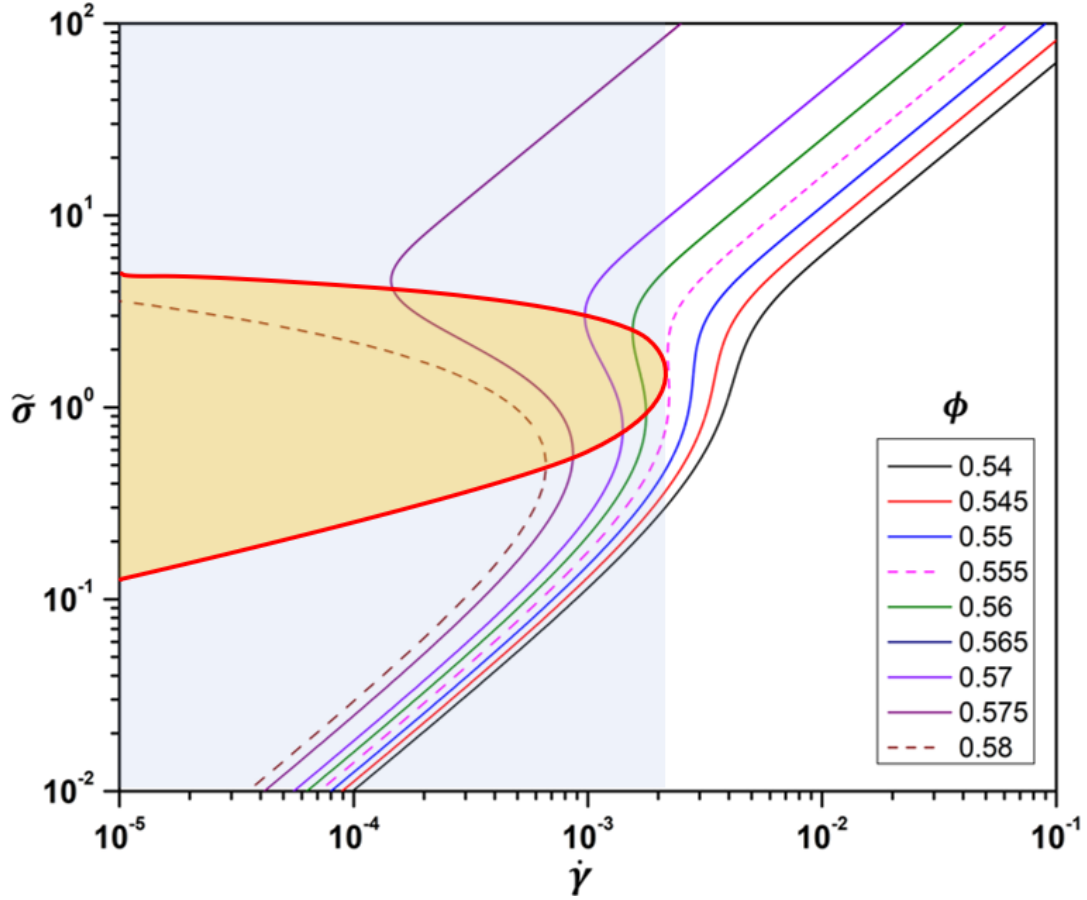
Figure 1.8: $\log(\tilde{\sigma})$ vs. $\log(\dot{\gamma})$ for $\phi_r = 0.58$ and $\phi_s = 0.64$. λ and σ^* are both taken as one with $f(\tilde{\sigma}) = 1 - e^{\tilde{\sigma}}$. With increase in ϕ, transition from CST to DST is observed with two regions separated by pink dashed curve corresponding to $\phi = 0.555$ (pink dashed curve). Yellow shaded region corresponds to unstable flow since η is negative in this region. Remade from [43].

.

curves corresponding to different ϕ is shown Figure 1.8. With ϕ, transition from CST to DST occurs at $\phi = 0.55$ which is less than ϕ_m and on increasing ϕ further, the curve starts bending backwards. For $\phi = \phi_m$, stable flow is observed only for small values of $\dot{\gamma}$, with viscosity diverging to infinity at higher σ.

1.4.4   Decoupling hydrodynamic interactions and frictional contacts contribution to ST in suspensions

In the previous subsections, two different mechanisms resulting in ST are explained. The first model relies on hydrodynamic interactions between the particles resulting in particle cluster formation, also observed experimentally (Figure 1.5 (c)) [24, 44]. While

the second model very well explains the discontinuous jump in η with $\dot{\gamma}$ at higher values of ϕ by taking inter-particle frictional contacts into account. In a suspension, both mechanisms contributes to η and resulting viscosity can be written as $\eta_{tot} = \eta_{hyd} + \eta_{fri}$. To decouple individual contributions to η, the time-reversal nature of the lubrication interactions in particle clusters can be utilized. If the flow direction is reversed instantly, only hydrodynamic contribution to η will remain and the frictional contribution will vanish. Figure 1.9 (a)-(b) displays results from an experiment that adopted instantaneous flow reversal strategy to decouple the hydrodynamic and frictional contribution to η. In there findings, hydrodynamic contribution to η, which corresponds to the observed viscosity at smaller values of strains (γ), remains almost constant with $\dot{\gamma}$. The major contribution to viscosity comes from the frictional contacts which grow with $\dot{\gamma}$ even in the CST regime [45].

Simulations based on hydrodynamic interactions suggests, formation of hydroclusters is accompanied by negative first normal stress difference (N_1) defined as

$$N_1 = \sigma_{xx} - \sigma_{yy} \qquad (1.19)$$

where σ_{ij} is the stress tensor with flow along x-direction and gradient along y. N_1 becomes increasingly negative with ϕ if hydrodynamic interaction dominates and positive when frictional force network dominates. Investigation of N_1 with σ reveals its transition from negative to positive values with increase in particle concentration [46], even though no CST to DST transition can be seen in the flow-curves (Figure 1.9 (c)-(d)). N_1 stays negative in moderately concentrated regime indicating masking of frictional contribution by hydrodynamic interactions. But as ϕ increases, force chain network dominates resulting in N_1 changing its sign to positive.

1.5 Flow instabilities in DST

Suspensions that undergo DST often display an S-shaped curve in stress-controlled experiments such that in the intermediate region $d\sigma/d\dot{\gamma} < 0$, indicating the presence of negative η [47]. In this region, $\dot{\gamma}$ becomes a multivalued function of σ, and shear-rate controlled measurements display flow hysteresis in the forward and reverse sweep measurements. The presence of negative slope indicates $\dot{\gamma}$ decreases on increasing σ and vice-versa, which is not possible experimentally. Because of this contradiction, flow instabilities are expected and already been well observed experimentally [47, 48]. Since the homogeneous flow is mechanically impossible in this region, one expects flow to be accompanied by the formation of steady shear-bands [49]. This possibility can be
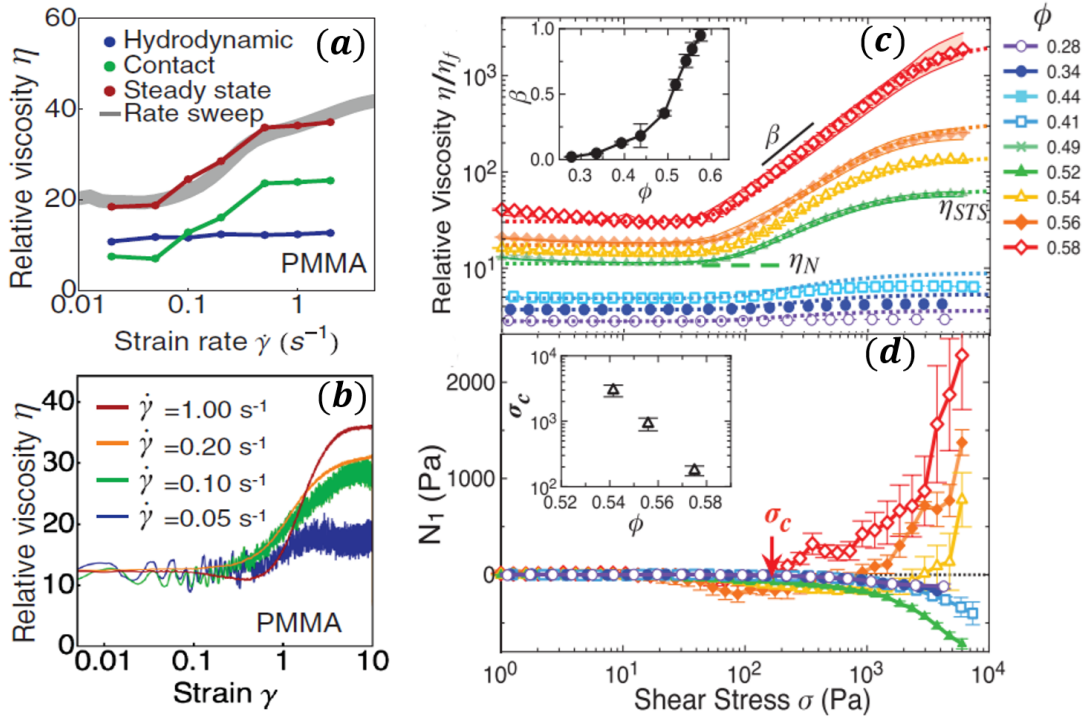
Figure 1.9: (a) Relative viscosity vs shear-rate measurement for PMMA particles for $\phi = 0.51$. Grey line corresponds to shear-rate sweep measurements, red curve corresponds to steady-state viscosity achieved while performing constant shear-rate reversal experiments, green and blue curve corresponds to frictional and hydrodynamic contribution to total viscosity. (b) Viscosity as a function of strain after the shear-reversal. At lower strains, only hydrodynamic interaction contributes to η, while both hydrodynamics and frictional interactions contribute to viscosity at higher strains. (c)-(d) corresponds to relative viscosity vs. stress and first stress difference (N_1) vs. stress for different volume fractions for silica particles. For $\phi > 0.54$, N_1 stays positive at higher stresses indicating dominating frictional contribution. (a)-(b) are adopted from [45] and (c)-(d) are adopted from [46] with permission

ruled out because of the requirement that solvent pressure and normal-normal particle stress component at the interface of the two bands must be balanced separately to avoid any unbalanced migration flux. Hence in DST, the flow is unsteady and exhibits rheochaos [50, 51]. These flow instabilities are accessed experimentally by performing stress-relaxation measurements, in which behavior of $\dot{\gamma}$ is observed with time (t) for a fixed value of σ. Flow is called steady if $\dot{\gamma}$ converges to a fixed value with time and unsteady if temporal rich dynamics are observed. In Figure 1.10, flow curve and stress relaxation measurements performed on a suspension of poly(methyl-methacrylate) particles (PMMA) of radius R=10μm suspended water mixture is shown [47]. For $\phi = 0.58$, an S-shaped curve can be seen, and the flow curve can be sub-divided into three different windows corresponding to Newtonian, intermediate, and shear-thickened states.
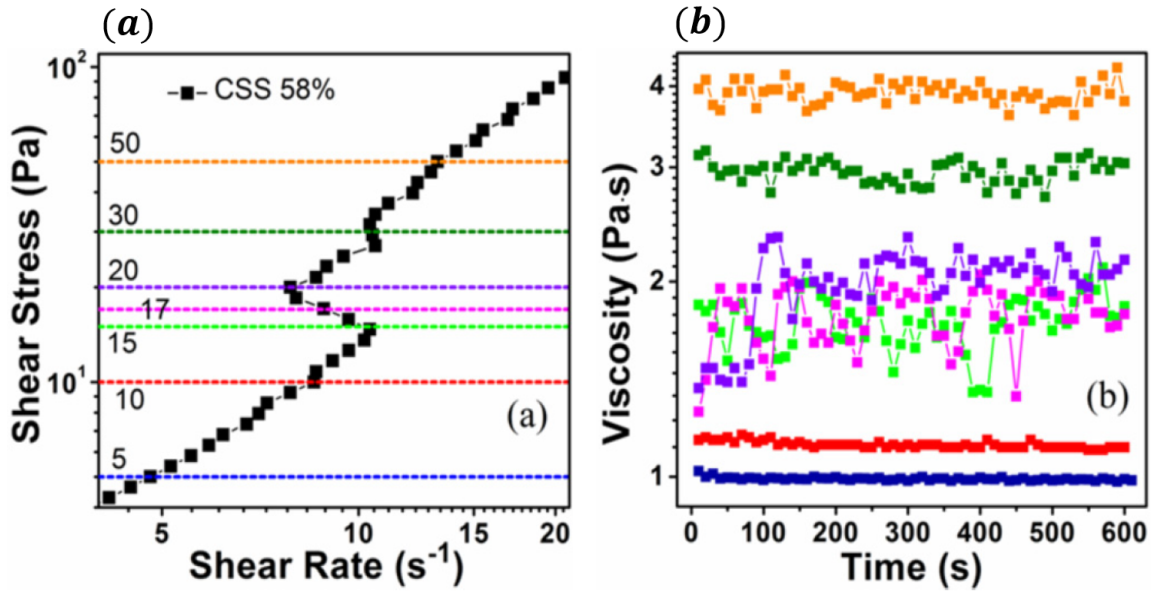
Figure 1.10: (a) Flow curve for a suspension of PMMA particles at $\phi = 0.58$. Horizontal dashed lines corresponds to stresses in three different regions of the curve: Newtonian (5, 10Pa), intermediate (15, 17, 20 Pa) and thickened state (30, 50Pa). (b) Stress-relaxation measurements at stresses indicated by same colour horizontal dashed lines in (a). (a) and (b) are Adopted from [47] with permission.

On imposing constant σ in either Newtonian or shear-thickened state, η remains almost constant for 600s. It suggests flow is stable in both of these regions. While in the intermediate state, η varies between 1.3 Pa.s and 2.5 Pa.s, indicating the coexistence of Newtonian and shear-thickened states.

Experiments performed on suspension of cornstarch at $\phi > \phi_m$, where ϕ_m is the jamming density defined in the Wyart and Cates model, display similar flow behavior except that there is no steady shear-thickened region (higher stress quasi-Newtonian region). For $\sigma < 0.1P^*$, where P^* is the onset pressure for the formation of frictional contacts, $\dot{\gamma}$ remains largely constant (Figure 1.11 (a)). On increasing σ further towards the discontinuity, jammed states start occurring rarely. This can be observed as a dip in $\dot{\gamma}$ with time in Figure 1.11 (b). For $\sigma \geqslant 0.2P^*$, the frequency of the jammed state becomes well defined. The frequency increases linearly with σ and at higher stresses transits from oscillatory to chaotic flow profile (Figure 1.11 (c)-(e)). Interestingly the normal force plotted as black curves in Figure 1.11 (b)-(e) also peaks whenever there is a decrease in $\dot{\gamma}$ indicating frictional interaction contribution to η.

In the CST regime, one does not expect flow instabilities since the slope of the flow curve always remains positive. But for anisotropic particulate suspensions, an extra degree of freedom may give rise to exotic flow behavior.
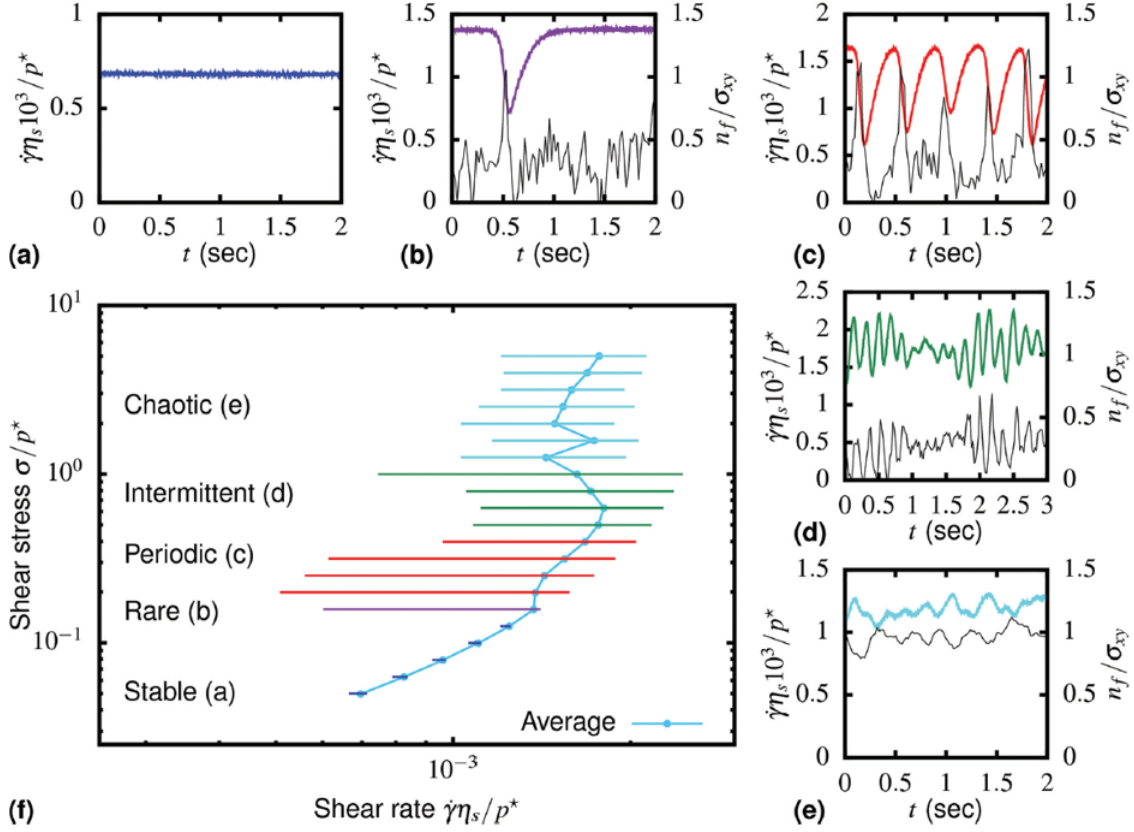
Figure 1.11: (a)-(e) Stress-relaxation curves for a suspension of cornstarch and water mixture at $\phi > \phi_m$. All five curves corresponds to the different stress regime in the flow curve shown in (f). All panels are adopted from [48] with permission.

1.6   Tuning shear thickening in suspensions

Owing to such fascinating flow behavior of shear thickening suspensions, these fluids are not only of interest in science and technology, but also in everyday life. These fluids are widely used for entertainment purposes, which involves people running and cycling on a pool filled with concentrated cornstarch and water mixture without sinking, and placing of such fluids on a sound emitting speaker only to see forming of complex structures, but also find a wide range of applications in shock or vibration absorbing machinery such as designing of flexible and efficient body armor, rotational break, vibration isolation in devices and impact resistance electrolyte for batteries [52, 53, 54, 55]. These fluids also give rise to unwanted effects, which involves decrease in efficiency of the industrial processes while handling such suspensions, for example, jamming of slurries during transportation via pipelines and mixing processes in food and cosmetic industries. Because of such a wide range of interests and applications, tuning ST in suspensions as per the need becomes essential. Our understanding of the ST mechanism suggests flow

behavior of ST fluid depends on ϕ, particle shape, and interparticle interactions. Hence by changing these parameters, one can tune suspension behavior.
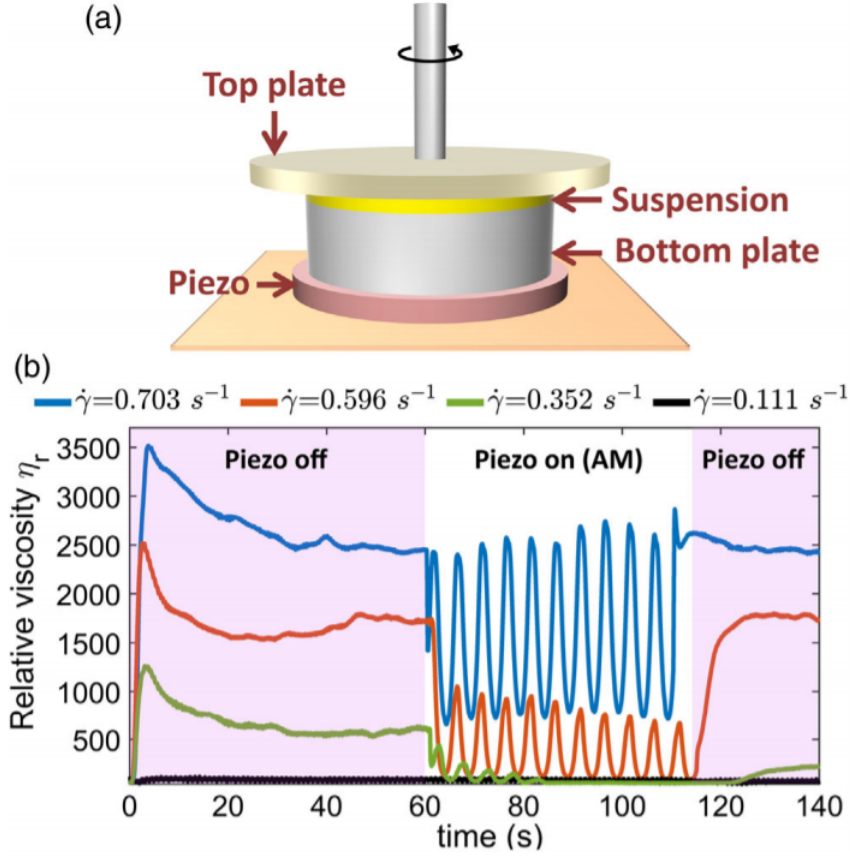
Figure 1.12: (a) Basic setup of an acoustic rheometer. The top plate is coupled to an external drive and is free to rotate while the bottom plate is fixed to a piezoelectric element. (b) Instantaneous value of η with time for a constant $\dot{\gamma}$. Confined sample consists to $2\mu m$ silica particles in dipropylene glycol and $\phi = 0.53$. Piezoelectric element vibrates at $f_z = 1.15MHz$ and amplitude modulated acoustic perturbation of frequency 0.2hz is applied at $t = 60s$. (a)-(b) are adopted from [56] with permission.

Suspensions containing anisotropic particles such as rods tend to show ST behavior at lower ϕ as compared to spherical particle suspensions. Since excluded volume increases with particle aspect ratio, both ST and shear-jamming volume fraction value also drops down considerably [23]. This may have significant implications in reducing the overall weight of ST based body armor. In industrial processes, changing the composition of the suspension is not feasible. Hence in such a scenario, tuning needs to be achieved by changing the external environment. According to the frictional model of shear thickening, force chain networks formation occurs at higher ϕ, resulting in shear-jamming or complete flow arrest (jamming of slurries). So if one could break the force chains network, lowering of η can be achieved. It can be done by providing ex-

ternal acoustic perturbation in the direction normal to the flow. Figure 1.12 (a) shows a method to provide acoustic amplitude-modulated perturbation in the flow-gradient direction using a piezoelectric crystal, and the corresponding plot shows η with time for different $\dot{\gamma}$. η oscillates at amplitude modulated wave frequency with the lowest value corresponding to the maximum amplitude (Figure 1.12 (b)). For this method to work, relative displacement generated by the perturbation should be greater than particle surface roughness scale and time scale faster than $1/\dot{\gamma}$ which is the turnover rate of the force chain network [56].
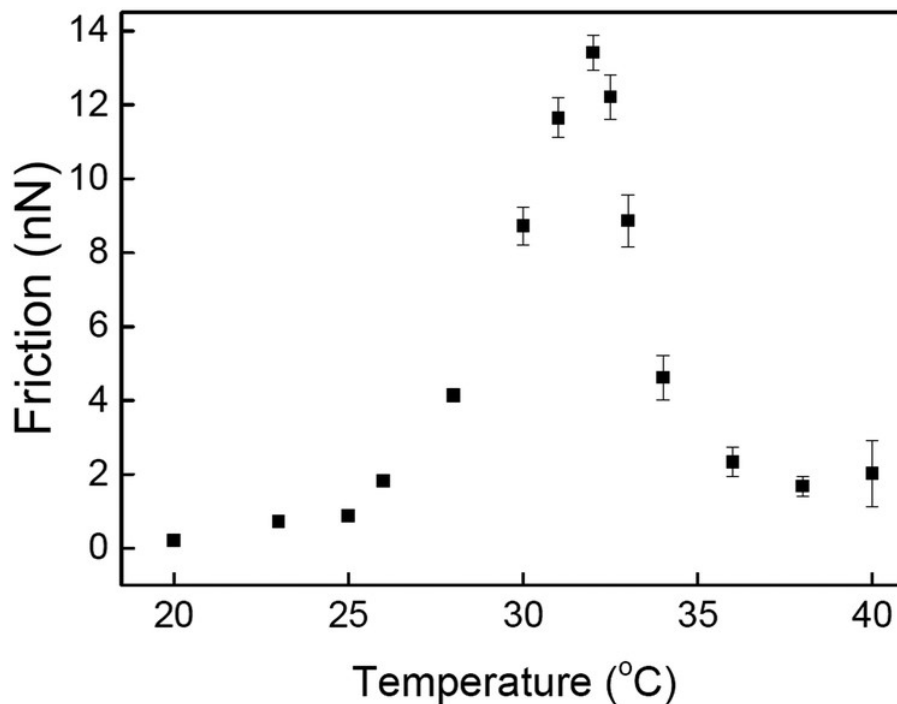
Figure 1.13: Frictional force vs temperature plot for a surface coated with PNIPAM polymer. Adopted from [58] with permission.

Another strategy to tune ST is by changing the inter-particle interactions. ST is not observed when particles have attractive interactions since frictional contacts are never absent, leading to a high value of yield stress. A good example is non-Brownian suspension of calcite particles suspended in glycerol-water mixture, which can be tuned from yield-stress suspension to ST suspension by the addition of surfactants such as polyacrylic acid sodium (PAA), Alkyl-naphthalene sulphonate condensate sodium salt (ANS), and Polycarboxylate ether (PCE) [57]. These attractive interactions arises due to finite residual van der Waals attraction, resulting from poor stabilization of the suspension. Such particles can form bonds with each other, and even for smaller values of σ can give rise to force bearing network resulting in higher than expected yield

stresses. Since inter-particle friction plays a role in ST, one can tune the ST exponent (β) just by making the particle surface either more rough or smooth, which can be achieved by chemically changing the surface tribology of the particles. One way to achieve it is by grafting stimulus-responsive polymer on the particles such as Poly(N-isopropylacrylamide) (PNIPAM), which is a temperature-sensitive polymer. Below the lower critical solvent temperature (T_{LCST}), polymer stays in the swollen form in an aqueous medium and switches to collapsed state above the lower critical solvent temperature. Near T_{LCST}, the partial collapse of the polymer results in stiffer surface asperities causing enhancement of surface friction (Figure 1.13) [58]. This transition of the polymer with temperature allows us to alter surface tribology in situ, and in our experiments, we have utilized this strategy to tune shear thickening in a suspension of PNIPAM coated colloidal silica rods suspended in water. The findings of our experiments are discussed in chapter 3.

Bibliography

[1] M. White Frank. *Fluid Mechanics.* McGraw-Hill, 1998.

[2] Norbert Willenbacher and Kristina Georgieva. Rheology of disperse systems. *Product design and engineering: Formulation of gels and pastes*, pages 7–49, 2013.

[3] Angelo Castruccio, AC Rust, and RSJ Sparks. Assessing lava flow evolution from post-eruption field data using herschel–bulkley rheology. *Journal of Volcanology and Geothermal Research*, 275:71–84, 2014.

[4] Philippe Coussot and Jean Michel Piau. On the behavior of fine mud suspensions. *Rheologica acta*, 33(3):175–184, 1994.

[5] F De Larrard, CF Ferraris, and T Sedran. Fresh concrete: a herschel-bulkley material. *Materi als and structures*, 31(7):494–498, 1998.

[6] R Tuinier, J Rieger, and CG De Kruif. Depletion-induced phase separation in colloid–polymer mixtures. *Advances in colloid and interface science*, 103(1):1–31, 2003.

[7] Hajime Tanaka, Yuya Nishikawa, and Takehito Koyama. Network-forming phase separation of colloidal suspensions. *Journal of Physics: Condensed Matter*, 17(15):L143, 2005.

[8] Hartmut Löwen. Possibilities of phase separation in colloidal suspensions. *Physica A: Statistical Mechanics and its Applications*, 235(1-2):129–141, 1997.

[9] DH Napper and A Netschey. Studies of the steric stabilization of colloidal particles. *Journal of Colloid and Interface Science*, 37(3):528–535, 1971.

[10] Ekaterina B Zhulina, Oleg V Borisov, and Victor A Priamitsyn. Theory of steric stabilization of colloid dispersions by grafted polymers. *Journal of colloid and interface science*, 137(2):495–511, 1990.

[11] Cristina Lourenco, Maribel Teixeira, Sérgio Simões, and Rogério Gaspar. Steric stabilization of nanoparticles: size and surface properties. *International journal of pharmaceutics*, 138(1):1–12, 1996.

[12] José Hierrezuelo, Amin Sadeghpour, Istvan Szilagyi, Andrea Vaccaro, and Michal Borkovec. Electrostatic stabilization of charged colloidal particles with adsorbed polyelectrolytes of opposite charge. *Langmuir*, 26(19):15109–15111, 2010.

[13] Jiwen Liu and Erik Luijten. Stabilization of colloidal suspensions by means of highly charged nanoparticles. *Physical Review Letters*, 93(24):247802, 2004.

[14] Anthony Stone. *The theory of intermolecular forces*. oUP oxford, 2013.

[15] EWJ Mardles. Viscosity of suspensions and the einstein equation. *Nature*, 145(3686):970–970, 1940.

[16] L Landau and LD See. Landau, em lifshitz, fluid mechanics, 1943.

[17] Kazem Bashirnezhad, Shahab Bazri, Mohammad Reza Safaei, Marjan Goodarzi, Mahidzal Dahari, Omid Mahian, Ahmet Selim Dalkılıça, and Somchai Wongwises. Viscosity of nanofluids: a review of recent experimental studies. *International Communications in Heat and Mass Transfer*, 73:114–123, 2016.

[18] G. K. Batchelor. *An introduction to fluid dynamics*. Cambridge University Press, 1967.

[19] John F Brady and Georges Bossis. The rheology of concentrated suspensions of spheres in simple shear flow by numerical simulation. *Journal of Fluid mechanics*, 155:105–129, 1985.

[20] Norman J Wagner and John F Brady. Shear thickening in colloidal dispersions. *Physics Today*, 62(10):27–32, 2009.

[21] SR Williams and AP Philipse. Random packings of spheres and spherocylinders simulated by mechanical contraction. *Physical Review E*, 67(5):051301, 2003.

[22] Nicole M James, Huayue Xue, Medha Goyal, and Heinrich M Jaeger. Controlling shear jamming in dense suspensions via the particle aspect ratio. *Soft matter*, 15(18):3649–3654, 2019.

[23] Eric Brown, Hanjun Zhang, Nicole A Forman, Benjamin W Maynor, Douglas E Betts, Joseph M DeSimone, and Heinrich M Jaeger. Shear thickening and jamming in densely packed suspensions of different particle shapes. *Physical Review E*, 84(3):031408, 2011.

[24] Xiang Cheng, Jonathan H McCoy, Jacob N Israelachvili, and Itai Cohen. Imaging the microscopic structure of shear thinning and thickening colloidal suspensions. *Science*, 333(6047):1276–1279, 2011.

[25] RL Hoffman. Discontinuous and dilatant viscosity behavior in concentrated suspensions. i. observation of a flow instability. *Transactions of the Society of Rheology*, 16(1):155–173, 1972.

[26] RL Hoffman. Discontinuous and dilatant viscosity behavior in concentrated suspensions. ii. theory and experimental tests. *Journal of Colloid and Interface Science*, 46(3):491–506, 1974.

[27] Jonathan J Stickel and Robert L Powell. Fluid mechanics and rheology of dense suspensions. *Annu. Rev. Fluid Mech.*, 37:129–149, 2005.

[28] Joseph M Brader. Nonlinear rheology of colloidal dispersions. *Journal of Physics: Condensed Matter*, 22(36):363101, 2010.

[29] Xinliang Xu, Stuart A Rice, and Aaron R Dinner. Relation between ordering and shear thinning in colloidal suspensions. *Proceedings of the National Academy of Sciences*, 110(10):3771–3776, 2013.

[30] Neil YC Lin, Christopher Ness, Michael E Cates, Jin Sun, and Itai Cohen. Tunable shear thickening in suspensions. *Proceedings of the National Academy of Sciences*, 113(39):10774–10778, 2016.

[31] Animesh Laha and Abhijit Majumdar. Interactive effects of p-aramid fabric structure and shear thickening fluid on impact resistance performance of soft armor materials. *Materials & Design*, 89:286–293, 2016.

[32] Selim Gürgen, Melih Cemal Kuşhan, and Weihua Li. Shear thickening fluids in protective applications: a review. *Progress in Polymer Science*, 75:48–72, 2017.

[33] RG Cox, IYZ Zia, and SG Mason. Particle motions in sheared suspensions xxv. streamlines around cylinders and spheres. *Journal of Colloid and Interface Science*, 27(1):7–18, 1968.

[34] Gaetano D'Avino, Martien A Hulsen, Frank Snijkers, Jan Vermant, Francesco Greco, and Pier Luca Maffettone. Rotation of a sphere in a viscoelastic liquid subjected to shear flow. part i: Simulation results. *Journal of rheology*, 52(6):1331–1346, 2008.

[35] Ryohei Seto, Romain Mari, Jeffrey F Morris, and Morton M Denn. Discontinuous shear thickening of frictional hard-sphere suspensions. *Physical review letters*, 111(21):218301, 2013.

[36] David R Foss and John F Brady. Structure, diffusion and rheology of brownian suspensions by stokesian dynamics simulation. *Journal of Fluid Mechanics*, 407:167–200, 2000.

[37] Ehssan Nazockdast and Jeffrey F Morris. Microstructural theory and the rheology of concentrated colloidal suspensions. *Journal of Fluid Mechanics*, 713:420, 2012.

[38] Chiao-Peng Hsu, Shivaprakash N Ramakrishna, Michele Zanini, Nicholas D Spencer, and Lucio Isa. Roughness-dependent tribology effects on discontinuous shear thickening. *Proceedings of the National Academy of Sciences*, 115(20):5117–5122, 2018.

[39] François Boyer, Élisabeth Guazzelli, and Olivier Pouliquen. Unifying suspension and granular rheology. *Physical review letters*, 107(18):188301, 2011.

[40] Yoël Forterre and Olivier Pouliquen. Flows of dense granular media. *Annu. Rev. Fluid Mech.*, 40:1–24, 2008.

[41] ME Cates, MD Haw, and CB Holmes. Dilatancy, jamming, and the physics of granulation. *Journal of Physics: Condensed Matter*, 17(24):S2517, 2005.

[42] Rut Besseling, Lucio Isa, Pierre Ballesta, G Petekidis, ME Cates, and WCK Poon. Shear banding and flow-concentration coupling in colloidal glasses. *Physical review letters*, 105(26):268301, 2010.

[43] Matthieu Wyart and ME Cates. Discontinuous shear thickening without inertia in dense non-brownian suspensions. *Physical review letters*, 112(9):098302, 2014.

[44] Dennis P Kalman and Norman J Wagner. Microstructure of shear-thickening concentrated suspensions determined by flow-usans. *Rheologica acta*, 48(8):897–908, 2009.

[45] Neil YC Lin, Ben M Guy, Michiel Hermes, Chris Ness, Jin Sun, Wilson CK Poon, and Itai Cohen. Hydrodynamic and contact contributions to continuous shear thickening in colloidal suspensions. *Physical review letters*, 115(22):228304, 2015.

[46] John R Royer, Daniel L Blair, and Steven D Hudson. Rheological signature of frictional interactions in shear thickening suspensions. *Physical review letters*, 116(18):188301, 2016.

[47] Zhongcheng Pan, Henri de Cagny, Bart Weber, and Daniel Bonn. S-shaped flow curves of shear thickening suspensions: Direct observation of frictional rheology. *Physical Review E*, 92(3):032202, 2015.

[48] Michiel Hermes, Ben M Guy, Wilson CK Poon, Guilhem Poy, Michael E Cates, and Matthieu Wyart. Unsteady flow and particle migration in dense, non-brownian suspensions. *Journal of Rheology*, 60(5):905–916, 2016.

[49] Peter D Olmsted. Perspectives on shear banding in complex fluids. *Rheologica Acta*, 47(3):283–300, 2008.

[50] Brice Saint-Michel, Thomas Gibaud, and Sébastien Manneville. Uncovering instabilities in the spatiotemporal dynamics of a shear-thickening cornstarch suspension. *Physical Review X*, 8(3):031006, 2018.

[51] Matthias Grob, Annette Zippelius, and Claus Heussinger. Rheological chaos of frictional grains. *Physical Review E*, 93(3):030901, 2016.

[52] NORMAN Wagner and E Wetzel. Advanced body armor utilizing shear thickening fluids. In *23rd Army Science Conference, Orlando, FL*, volume 3, 2002.

[53] Tongfei Tian and Masami Nakano. Design and testing of a rotational brake with shear thickening fluids. *Smart Materials and Structures*, 26(3):035038, 2017.

[54] Péter Nagy-György and Csaba Hős. Predicting the damping characteristics of vibration dampers employing generalized shear thickening fluids. *Journal of Sound and Vibration*, 506:116116, 2021.

[55] Gabriel M Veith, Beth L Armstrong, Hsin Wang, Sergiy Kalnaus, Wyatt E Tenhaeff, and Mary L Patterson. Shear thickening electrolytes for high impact resistant batteries. *ACS Energy Letters*, 2(9):2084–2088, 2017.

[56] Prateek Sehgal, Meera Ramaswamy, Itai Cohen, and Brian J Kirby. Using acoustic perturbations to dynamically tune shear thickening in colloidal suspensions. *Physical review letters*, 123(12):128001, 2019.

[57] James A Richards, Rory E O'Neill, and Wilson CK Poon. Turning a yield-stress calcite suspension into a shear-thickening one by tuning inter-particle friction. *Rheologica Acta*, 60(2):97–106, 2021.

[58] Yunlong Yu, Bernard D Kieviet, Fei Liu, Igor Siretanu, Edit Kutnyánszky, G Julius Vancso, and Sissi de Beer. Stretching of collapsed polymers causes an enhanced

dissipative response of pnipam brushes near their lcst. *Soft Matter*, 11(43):8508–8516, 2015.

Chapter 2

Experimental details

This chapter describes experimental details and techniques used to investigate the flow properties of the colloidal suspension and is divided into three sections. The first section provides details of the rheometer, the measuring geometries used to carry out flow measurements, and the inverted microscope, which is coupled to optical tweezers to investigate inter–particle surface friction with temperature. The second section describes protocols followed to synthesize colloidal silica particles and coat them with temperature-sensitive polymer brushes via well-established routes. The last section describes step-wise methods and procedures followed to perform the experiments.

Rheology is a science which deals with the deformation of materials, both solid or liquid, and a rheometer is a device used to obtain these insights. Rheometer consists of an external drive to which various measuring geometries can be attached as per the requirement. The confinement of the sample and the flow profile in the gap depends on measuring geometry selection. The rheological properties of the sample are determined by providing torque using an external drive and analyzing the response of the coupled measuring system. In our case, we have used an MCR-702 rheometer with parallel-plate (PP) and cone-plate (CP) as measuring geometries [1].

Synthesis of silica colloidal rods was carried out using a single pot method followed by few cycles of cleaning of obtained particles in ethanol and then in water. The polydispersity was improved by letting the particles sediment overnight to separate smaller particles from larger ones. These rods were then used for flow-instability measurements. For the second part of the project, the same protocols were followed to obtain a new batch of colloidal rods, which were then coated with temperature-sensitive PNIPAM brushes by a two-step method: functionalization of particle surface and growing PNIPAM brushes on them. These particles were later on used for temperature-sensitive flow measurements.

Vertical position adjuster

Motor location

Quick fitting coupling and measuring sytem detection

Peltier controlled hood

Lower measuring plate

Anton Paar MCR 702 Rheometer
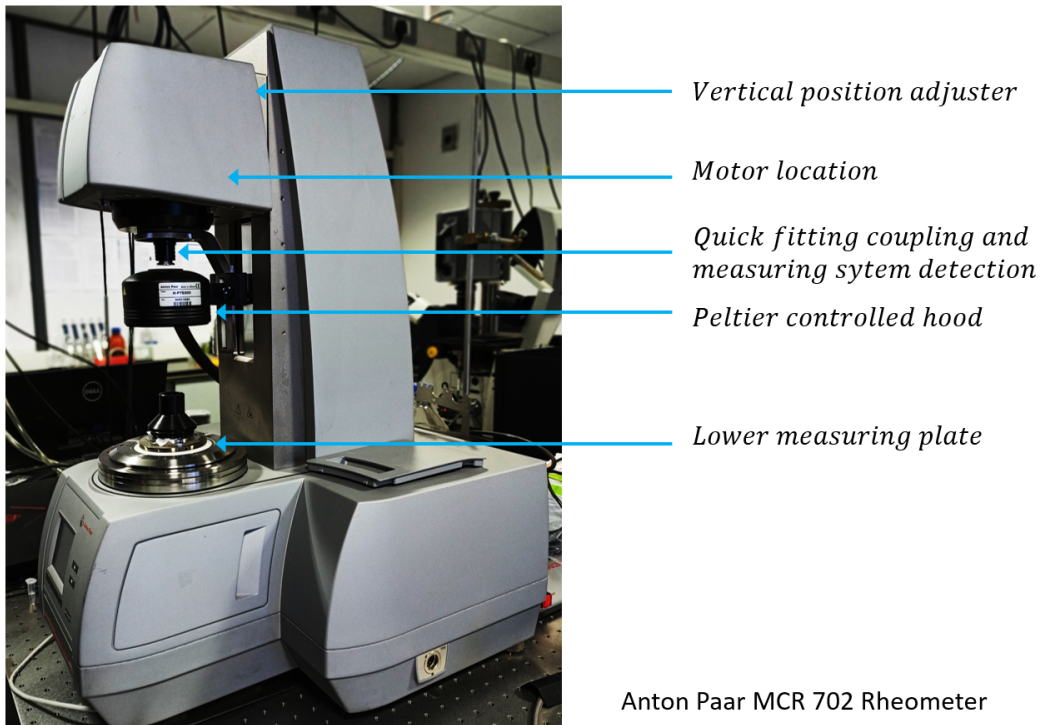
Figure 2.1: Image of Anton Paar MCR 702 rheometer used for all flow measurements.

2.1 Experimental setup

2.1.1 Rheometer and measuring geometries

For our experiments, we have used Anton Par MCR 702 rheometer (Figure 2.1). It comes equipped with an upper drive but can also be equipped with an additional lower drive that can rotate in a counterclockwise direction, allowing a stagnant plane formation, where particle dynamics can be imaged even at low frame rates. The motors are supported by two air bearings: a radial air bearing for center correction and stabilization and an axial bearing to hold the weight of rotating part. Sensors to measure normal forces are integrated with the air bearings and in addition, can be utilized for materials penetration tests. The drive features a linear relationship between torque and current, with the lowest possible torque being 0.5 nNm, the highest being 230 mNm, and the smallest possible angular deflection being 50 nrad. Three piezo elements are located in the measuring chamber reception to compensate for changes as low as 10nm in the gap because of fluctuations in temperature or other external factors. The device

is operated using Rheocompass, user-friendly software that provides predefined measurement templates and real-time data plotting, automation of tasks, and analysis.

To investigate the flow behavior of our sample, we have used two different geometries.

- **Cone-plate geometry**:

  In a cone-plate geometry (CP), sample is confined between a cone and a plate as illustrated in Figure 2.2 (a). To study the flow behavior, an external torque(M) is applied to the cone to make it rotate along a fixed axis while the other plate is kept stationary. The cone is truncated at the vertex for two reasons: to avoid contact friction between the cone tip and the plate, and to avoid damage to the cone during initial calibration and zero gapping. Cone angle is generally kept less than $4°$ which ensures that shear-rate is constant throughout the shearing gap [2]. The stress tensor, shear-rate and velocity profile in spherical polar coordinates for this geometry are expressed as:

$$\overline{\overline{\sigma}} = \begin{bmatrix} \sigma_{rr} & 0 & 0 \\ 0 & \sigma_{\theta\theta} & \sigma_{\theta\phi} \\ 0 & \sigma_{\phi\theta} & \sigma_{\phi\phi} \end{bmatrix} \; ; \; \dot{\gamma} = \frac{\Omega}{\alpha} \; ; \; v_\phi = \begin{bmatrix} 0 \\ 0 \\ \frac{r\Omega}{\alpha}\left(\frac{\pi}{2} - \theta\right) \end{bmatrix} \qquad (2.1)$$

  where 'r' is the radial distance measured from the bottom plate center .

  First normal stress difference defined as $N_1 = \sigma_{\phi\phi} - \sigma_{\theta\theta}$ for CP configuration is given by

$$N_1 = \frac{2F_Z}{\pi R^2} \qquad (2.2)$$

  where F_z is the normal force which can be directly measured by the rheometer. For our experiments we have used Quartz cone 25 mm diameter with cone angle as $0.979\,\mathrm{deg}$ and truncation of 48 μm. The bottom plate is of stainless steel (Figure 2.2 (c)).

- **Parallel-plate geometry**:

  In a parallel-plate geometry (PP), sample is confined between two circular parallel plates and torque is applied to one of the plate while the other plate is kept stationary (Figure 2.2 (b)). Relevant choice of coordinates for the geometry is cylindrical polar, with z-axis lying along the axis of rotation. Velocity is directed along the $\hat{\phi}$ with gradient along both the z and the radial direction. Stress tenor,
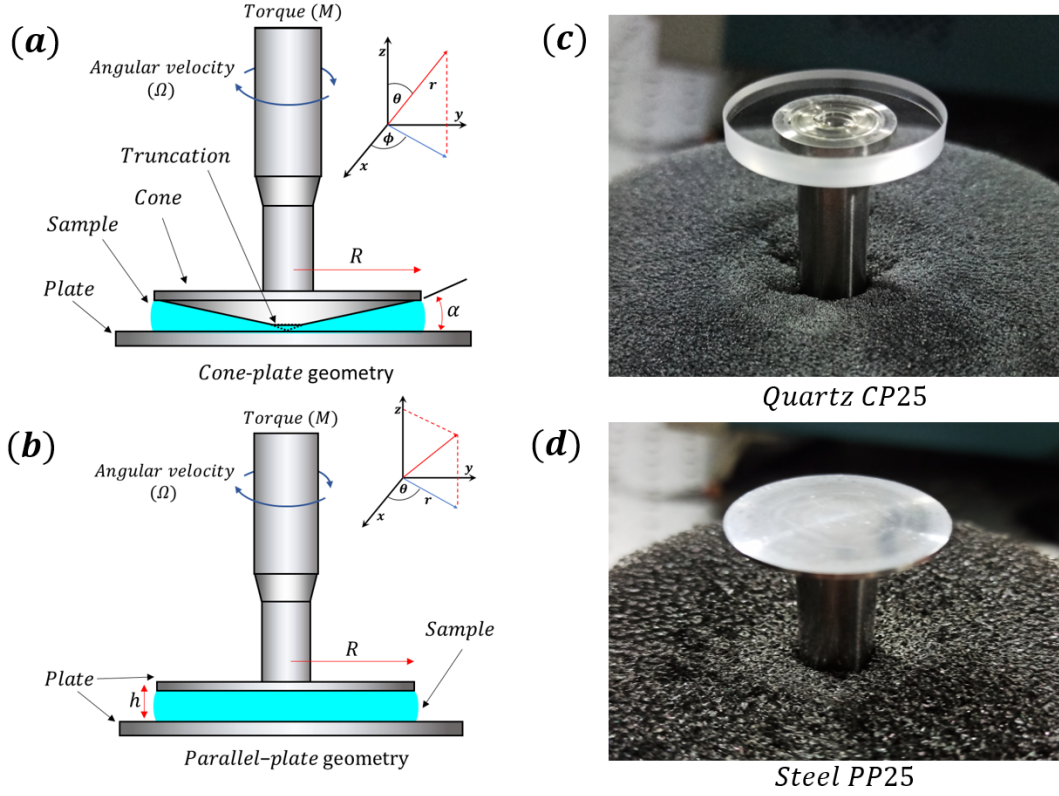
Figure 2.2: (a) and (b) are schematics of cone-plate and parallel-plate measuring systems. (c) and (d) are actual images of the quartz-cone and the steel top plate used in experiments.

shear-rate and velocity profile for a PP can be written as:

$$\overline{\overline{\sigma}} = \begin{bmatrix} \sigma_{rr} & 0 & 0 \\ 0 & \sigma_{\theta\theta} & \sigma_{\theta z} \\ 0 & \sigma_{z\theta} & \sigma_{zz} \end{bmatrix} \; ; \; \dot{\gamma} = \frac{r\Omega}{h} \; ; \; v_\theta = \begin{bmatrix} 0 \\ \frac{r\Omega z}{h} \\ 0 \end{bmatrix} \tag{2.3}$$

In PP configuration total thrust depends on both first and seconds normal stress differences. $N_1 - N_2$ is given by

$$(N_1 - N_2)|_{\dot{\gamma}_R} = \frac{F_z}{\pi R^2}\Big(2 + \frac{dln(Fz)}{dln\dot{\gamma}_R}\Big) \tag{2.4}$$

For accurate evaluation of $N_1 - N_2$, F_z along with its derivative with respect to $\dot{\gamma}$ needs to be determined. In general practice, N_1 is obtained using CP, and N_2 is determined using equation 2.4. In our experiments, we have used stainless steel
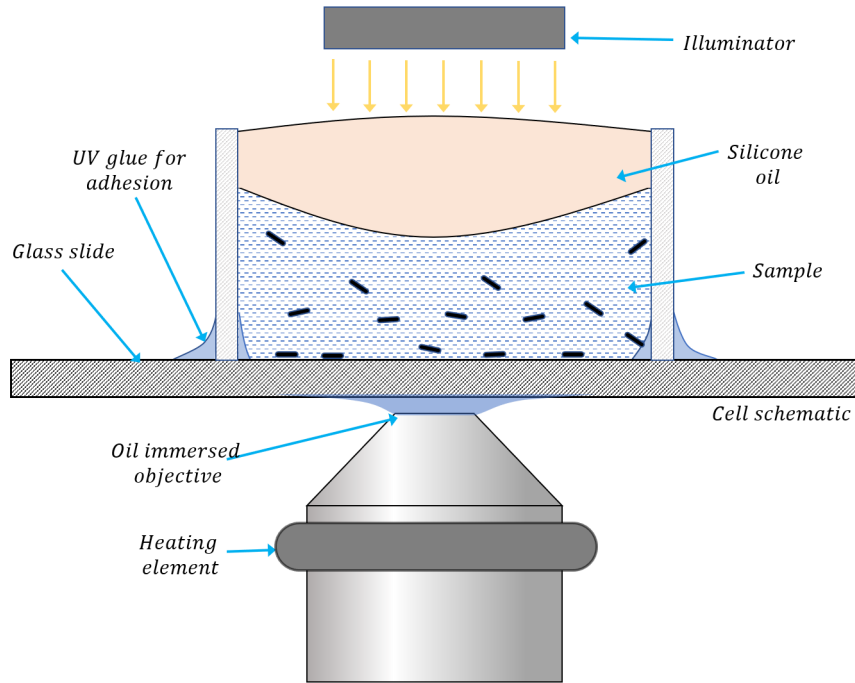
Figure 2.3: Schematic of the apparatus used for microscopic investigation of inter-particle surface interactions of a dimer with temperature.

plates of 25mm diameter (Figure 2.2 (d)).

A Peltier system is utilized to control the temperature in confinement, which is coupled to external water circulating chiller. The temperature of the circulating water is always set 5° below the desired temperature of the sample.

2.1.2   Inverted microscope and optical tweezers

To check particles after synthesis and obtain microscopic insight into the role of inter-particle surface frictions in ST, we used an inverted microscope by Leica (DM13000B) coupled to a 5 W laser (ALS-IR-5-SF) of wavelength $\lambda =$1065 nm. The power of the laser is set to 0.65 W, which is focused by the microscope's objective. This focused beam is then utilized for trapping and manipulating colloidal rods [3]. For all such experiments, we have used custom-made cells constructed out of sliced pipette tips pasted on a glass slide using UV curable glue (NOA81). For inter-particle friction-related experiments, sample (Polymer coated silica particles) is taken in a very dilute limit in Milli-Q water such that only a few particles are present in the field of view at

Figure 2.4: Image of synthesized colloidal silica rods under the microscope

a time. Silicone oil is added on top to avoid contamination of the sample and water evaporation during measurements (Figure 2.3).

2.2   Synthesis

2.2.1   Synthesis of colloidal silica rods

To synthesize colloidal rods, 30 gms of Polyvinylpyrrolidone (PVP) was measured and dissolved in 300ml of pentanol by sonicating the contents for at least 2 hours. Once all the PVP was dissolved, 30ml of ethanol, 8.4ml of Milli-Q water, and 2 ml of 0.18M solution of sodium citrate were added. The contents were mixed using the vortex method followed by sonication for 8 minutes. 6.75 ml of 25% ammonia solution was added, and the contents were mixed again. Finally, 3 ml of TEOS was added and remixed before keeping the flask in the oven overnight at 30°C. Once the reaction was complete, contents were centrifuged at 6000rpm to separate the rods. Lastly, rods were cleaned multiple times with ethanol to get rid of pentanol and then with water to replace ethanol. Obtained rods were then analyzed under a microscope, and their diameters were found to be between ≈ 0.6 and $0.8\mu m$ and length ≈ 3 to $6\mu m$ (Figure 2.4) [4].

2.2.2 Synthesis of P-NIPAM coated silica colloidal rods

Coating temperature-sensitive PNIPAM brushes on colloidal silica rods is a two-step process. About 250 μl of pure silica rods were taken in a 50ml vial and cleaned with Milli-Q water followed by ethanol 3-4 times. Excess ethanol was removed before starting the functionalization process, and the overall sample volume (ethanol + silica rods) was reduced to 20 ml. This sample was then transferred to a conical flask and 5 ml of Milli-Q water, 1 ml of 25% ammonia and 10 μl of 3-methacryloxypropyltrimethoxysilane (MPS) were added to the flask in sequence. The amount of MPS added is such that ~40μl is available for functionalization per square meter surface area of silica particles. The mixture was stirred continuously at 250rpm using a magnetic stirrer while maintaining the temperature at 27°C for 17 hours. The functionalized particles were then transferred back to 50 μl vial, cleaned with ethanol, and then with water 3-4 times. The total volume of functionalized particles + water was made to be 47.5 ml, and the mixture was taken in a round bottom flask placed on an oil bath. To maintain the inert environment inside the flask, nitrogen gas is made continuously bubble through the mixture. 0.3425 gms of N-isopropylacrylamide (NIPAM) and 0.0085 gms of N,N'-methylenebisacrylamide (BIS) were then added to the RB flask, and the mixture was heated to 70°C while stirring it continuously at 200rpm. Another magnetic stirrer was placed inside the oil bath to homogenize the oil temperature. Once the mixture temperature reached 70°C, polymerization initiator potassium persulfate (KPS) was added after an hour to the flask. The reaction was made to take place for 4 hours, after which the contents of the flask were transferred to a vial and were cleaned 5-6 times with Milli-Q water to separate surface-modified PNIPAM coated silica rods [5, 6]. These rods were then used for temperature-controlled rheology.

2.3

2.3.1 Cleaning of particles

To clean the silica particles after synthesis or during intermediate steps, particles were taken in a 50 ml centrifuge vial. The contents were then centrifuged at ≈6000 rpm for half an hour or longer. Once all the particles settled down at the bottom of the vial, the supernatant was removed carefully using a pipette without disturbing the particles at the bottom and is replaced with either fresh ethanol or Milli-Q water. The particles are then resuspended in a new medium by vortexing and sonicating the sample. Once all particles have resuspended, contents are again centrifuged, and the cycle is repeated

3-4 times or as required. For PNIPAM coated particles, cleaning is carried out only with water, and the vortex method is used for resuspending particles as sonication may cause the breaking of bonds, thereby damaging the polymer layer. Also, the centrifuge is carried out at less than 1500 rpm.

2.3.2   Determination of suspension volume fraction

To determine the total volume occupied by the particles, density of the supernatant (ρ_s), density of silica particles (ρ_p) and total volume of the suspension (V) needs to be determined. Density of the suspending medium and particles can be obtained directly from the literature and total volume can be determined either by using measuring cylinder or any other methods. In our experiements, we have used density of silica as 2.06 gms/ml. Now if V_p and V_s are the supernatant and total particle volume, then we have:

$$V_p + V_s = V$$
$$\rho_p V_p + \rho_s V_s = W$$

$$(2.5)$$

where W is the total weight of the suspension which can be directly determined using a weighing balance. Simplifying equation 2.5, one can rewrite V_p as:

$$V_p = \frac{W - \rho_s V}{\rho_p - \rho_s} \tag{2.6}$$

Once V_p is known, V_s can be determined using equation 2.5. Depending on the desired volume fraction ϕ, the amount of supernatant to be removed or added can be calculated as:

$$\triangle V_s = V - \frac{V_p}{\phi} \tag{2.7}$$

where $\triangle V_s$ is +ve if supernatant needs to be removed and -ve if it needs to be added. This calculation cannot be used for NIPAM coated particles since the effective volume, and density of particles changes because of the polymer layer and become a function of temperature and suspending medium.

2.3.3   Operation protocols for rheometer

An external compressor is turned on first for the functioning of air bearings in the rheometer (pressure >5 bar). Once the rheometer has turned on and initialized successfully using rheocompass software, calibration for the upper drive inertia is performed

*Quartz CP*25

Silicone oil

Encasing to hold oil and avoid sample evaporation

*Sample seeping out when the geometry is lowered to final position*
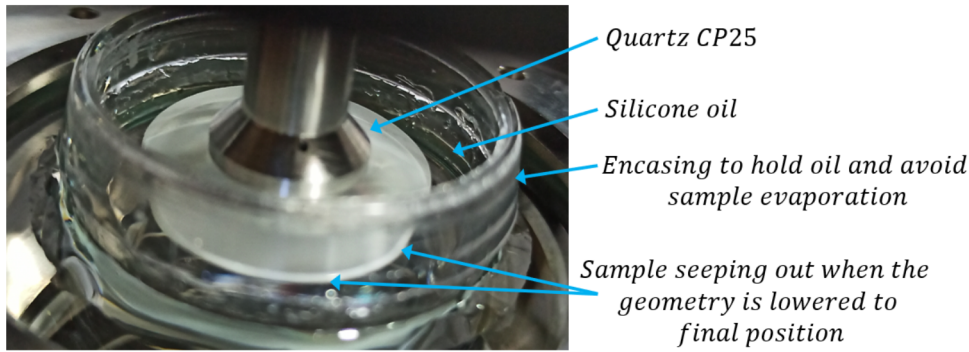
Figure 2.5: Image of PNIPAM coated rods suspension in water confined in a quartz cone and a glass plate geometry. The bottom plate is of glass customized by fixing a plastic boundary so that it can hold silicone oil. The white coloured sample can be seen seeping out of the gap signifying proper loading.

repeatedly unless no significant changes in initial and updated inertia are observed. After successful calibration of upper drive inertia, measuring geometry is attached to the drive, and zero gaping is performed. The calibration of measuring system inertia is performed multiple times at a 1 mm gap. The whole calibration procedure takes at least 1 hour and is essential to perform every time the rheometer is turned on, or new sets of measurements are performed. Lastly, motor adjustment is performed 2-3 times, and then the geometry is lifted so that the sample can be loaded. The amount of sample to be loaded depends on the attached geometry. For quartz CP-25, we loaded 85 μl, and for PP-25, we used 45 μl of sample for 65 μm gap, which was later lowered to 35 μm for another set of measurements. To ensure uniform spreading of the sample in the gap, geometry was lowered carefully in small discrete steps. The final investigation of the proper loading was ensured by visual inspection [7]. Silicone oil was used to confine the sample to avoid evaporation, and the region around the sample and the measuring geometry were enclosed in a Peltier-controlled hood (Figure 2.5). All the flow measurements are performed in this configuration.

2.3.4 Inter-particle surface friction experiments

For these experiments, a dilute sample of PNIPAM coated silica rods in water was taken in a vial, and sodium carboxymethyl cellulose (NaCMC) was added, thereby introducing attractive depletion interaction between the rods. The amount of NaCMC added was such that its final concentration in suspension is 0.05mg/ml. 50 μl of this

sample was carefully loaded in a cell and then confined with silicone oil from above. After an hour, few particles sedimented and aligned to the glass-slide plane because of the depletion interactions between the particles and the glass surface. Once enough particles settled down, we turned on the tweezers and brought rods of similar lengths together to form a dimer. The temperature of the cell was varied from 30°C to 34° using a temperature probe connected to the microscope objective (Figure 2.3). Lastly, an image sensor attached to a microscope was utilized to capture and record dimer dynamics, and further analysis was carried out using ImageJ and Matlab.

Bibliography

[1] Anand U Oza and David C Venerus. The dynamics of parallel-plate and cone–plate flows. *Physics of Fluids*, 33(2):023102, 2021.

[2] PR Williams. Rheometry for non-newtonian fluids. *In Non-Newtonian flow in the process industries Fundamentals and engineering applications*, pages 37–72, 1999.

[3] Arthur Ashkin. Optical trapping and manipulation of neutral particles using lasers. *Proceedings of the National Academy of Sciences*, 94(10):4853–4860, 1997.

[4] Anke Kuijk, Alfons Van Blaaderen, and Arnout Imhof. Synthesis of monodisperse, rodlike silica colloids with tunable aspect ratio. *Journal of the American Chemical Society*, 133(8):2346–2349, 2011.

[5] Jia Guo, Wuli Yang, Changchun Wang, Jia He, and Jiyao Chen. Poly (n-isopropylacrylamide)-coated luminescent/magnetic silica microspheres: preparation, characterization, and biomedical applications. *Chemistry of Materials*, 18(23):5554–5562, 2006.

[6] Zhimin Xing, Congling Wang, Jie Yan, Li Zhang, Lan Li, and Liusheng Zha. Dual stimuli responsive hollow nanogels with ipn structure for temperature controlling drug loading and ph triggering drug release. *Soft Matter*, 7(18):7992–7997, 2011.

[7] Leo H O Hellström, Mohamed A Samaha, Karen M Wang, Alexander J Smits, and Marcus Hultmark. Errors in parallel-plate and cone-plate rheometer measurements due to sample underfill. *Measurement Science and Technology*, 26(1):015301, 2014.

Chapter 3

Results and discussion

This chapter discusses the results and findings of our experiments with colloidal silica rods and PNIPAM coated silica rods suspensions. The chapter is divided into two subsections. In the first section, we have utilized a strategy to tune shear thickening (ST) by changing the surface tribology of the suspending particles. For this purpose, particles are coated with a temperature-sensitive polymer and suspended in water. Results from the rheological studies carried out on this sample followed by a microscopic investigation of dynamics of rods with temperature are presented in this section. In the second section, the suspension of colloidal silica rods in a 15:85 glycerol mixture is investigated in the continuous shear thickening (CST) regime. Stress relaxation measurements are performed to investigate the flow characteristics and to uncover any instabilities.

3.1 Flow behavior of PNIPAM coated silica rods suspension

Recent advancements in our understanding of the underlying mechanism resulting in ST indicate the importance of inter-particle frictional contacts in a suspension under shear [1, 2, 3]. To isolate the effect of friction during ST, the surface tribology of the suspending particles needs to be altered as a response to an easily controllable external stimulus. One such way is by grafting stimulus-responsive polymers on the surface of the particles such as Poly(N-isopropyl acrylamide) (PNIPAM). PNIPAM is a temperature-sensitive polymer that switches from an expanded state in an aqueous medium below lower critical solution temperature (LCST) to a collapsed state above LCST and can be further tuned by changing the pH or the solvent composition [4]. In our experiments, we restrict our attention to situations where external temperature
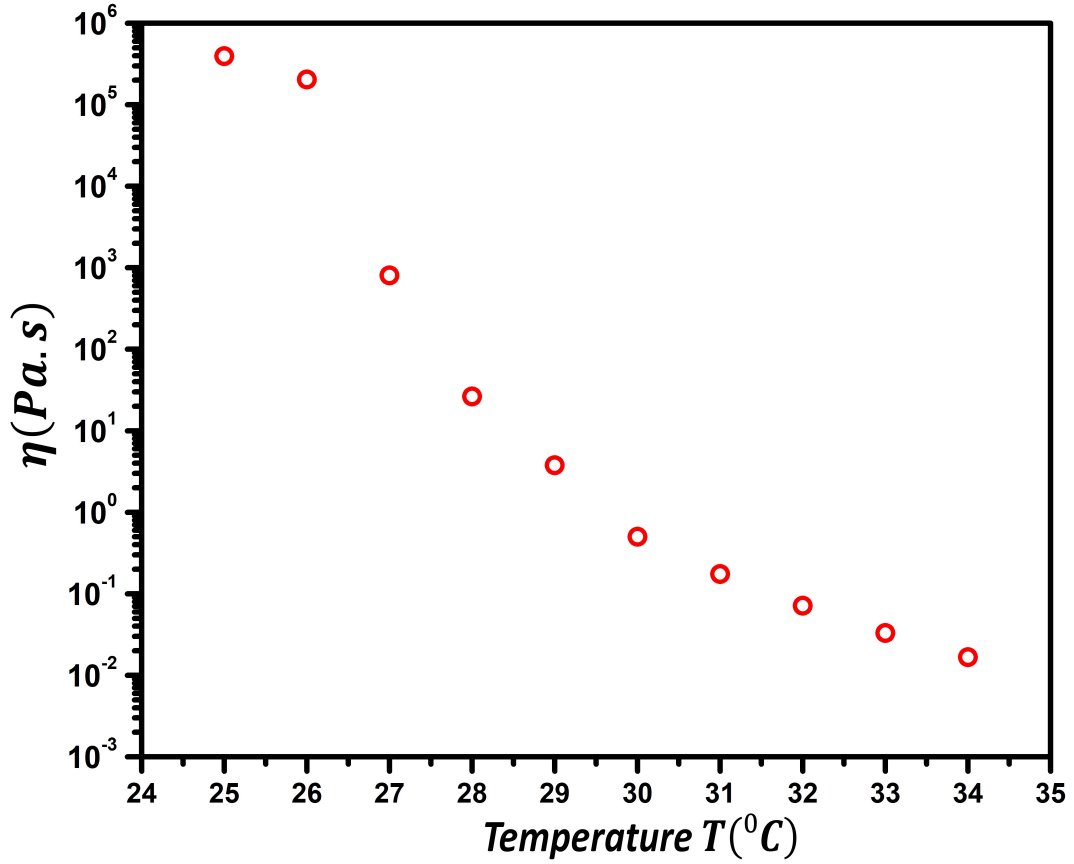
Figure 3.1: η as a function of T for $\sigma = 20$ Pa. With increase in T, η decreases because of collapse of PNIPAM brushes thereby decreasing the volume fraction of the suspension.

(T) is the stimuli. Along with the change in volume, the transition with temperature is followed by a non-monotonic change in friction μ [5, 6]. On approaching T_{LCST} from below, partial collapse of the brushes leads to the formation of stiffer surface asperities, resulting in enhancement of μ by an order of magnitude [5]. Beyond T_{LCST}, surfaces interact via hydrophobic interaction and adhere to each other. For our experiments, we have synthesized colloidal silica rods of diameter 0.6-0.8 μm, length 3-6 μm and grafted polymer brushes on them using established routes [7, 8, 9]. Surface-modified rods were taken in a vial and suspended in an aqueous medium. The vial was centrifuged, and excess water was removed using a pipette to obtain a concentrated suspension. Temperature ramp experiments at $\sigma = 20$ Pa were performed using Quartz cone with bottom plate made up of glass, and the corresponding results are shown in Figure 3.1. With T, the collapse of the polymer brushes results in lowering the effective volume

occupied by the particles. This decrease in ϕ causes η to decrease by about seven orders of magnitude when temperature is raised from 25°C to 34°C in steps of 1°C (Figure 3.1), verifying the success of PNIPAM grafting procedure.

3.1.1 Effect of temperature on shear thickening

For the flow curve (FC) measurements, we started with a highly concentrated sample (ϕ_6),which is prepared be centrifuging the vial containing sample at 1500 rpm and removing the excess supernatant using a pipette. The grafting of PNIPAM polymers on the particles makes their surfaces soft, which makes determination of volume fraction challenging.
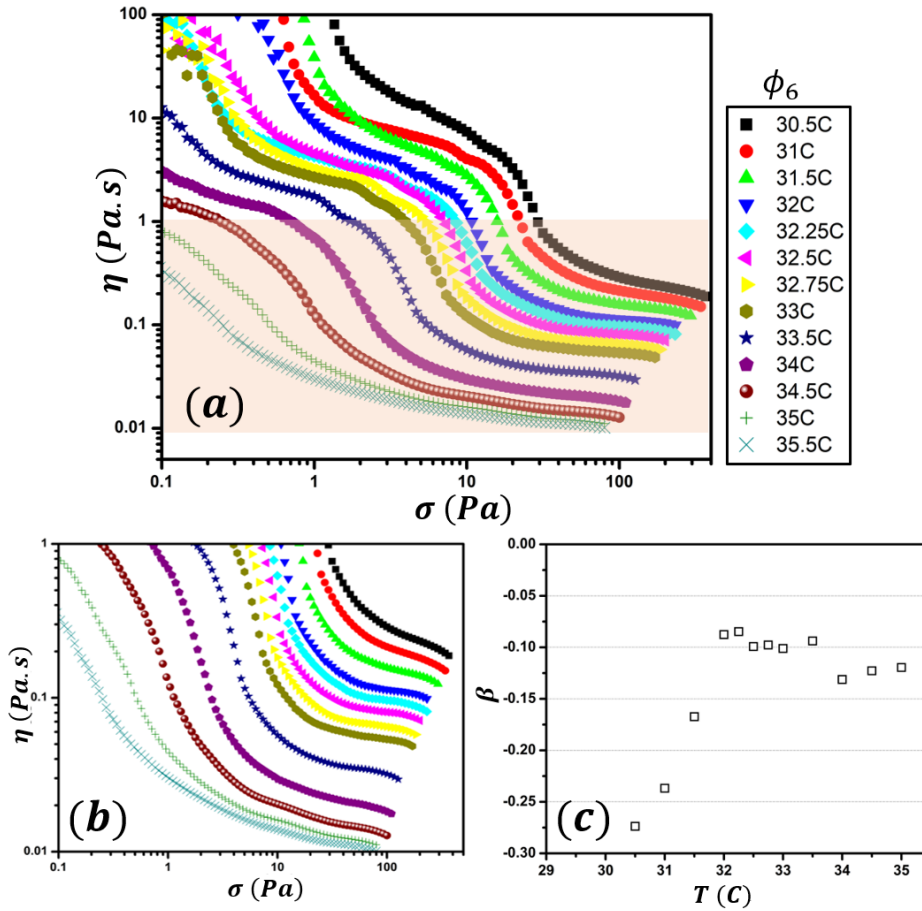
Figure 3.2: (a) η vs σ plots for ϕ_6 at different temperatures. (b) Zoomed in plot of the shaded region in (a). (c) β vs T plot, where β is the shear-thickening exponent. With T, β also increase but saturates to a non-positive value indicating suspension is shear thinning at all measured temperatures.
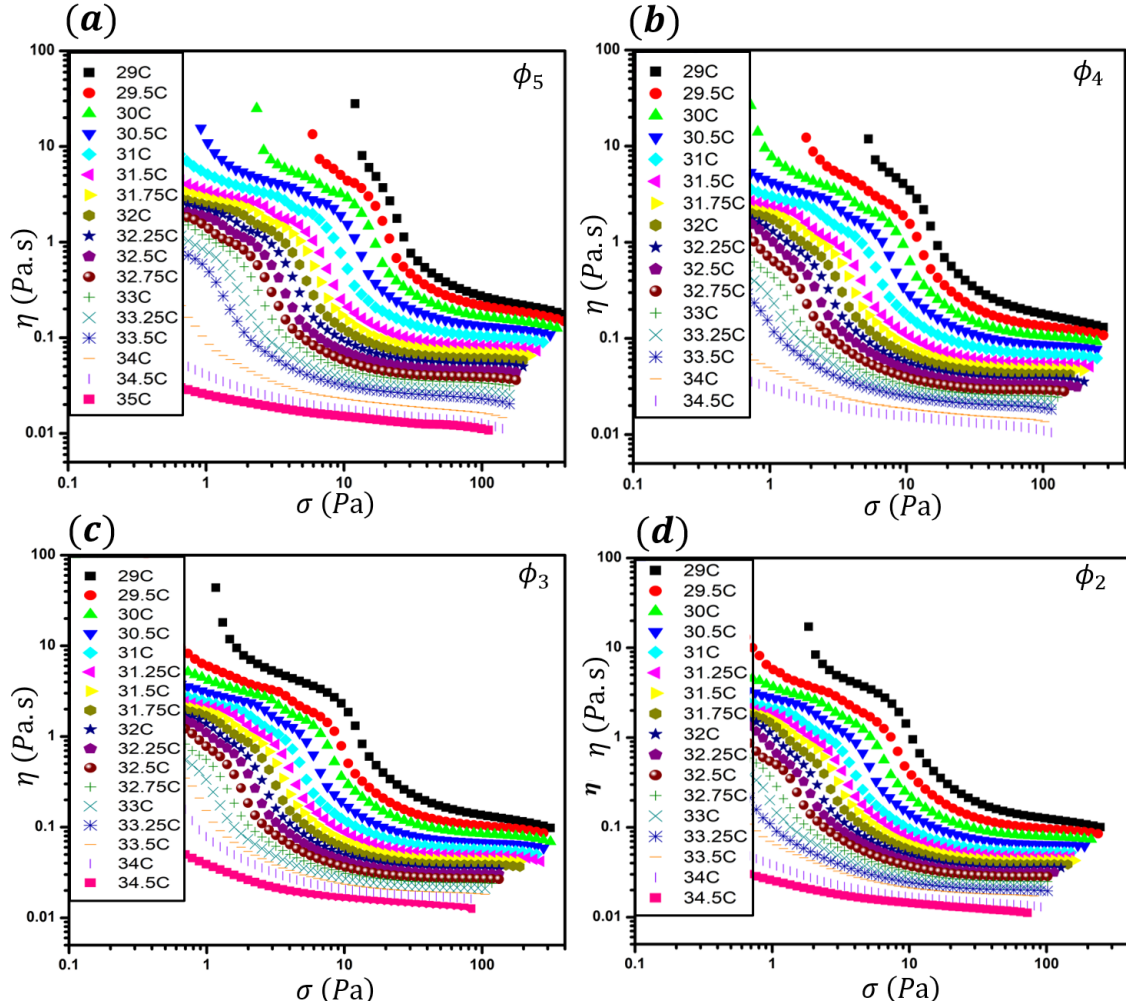
Figure 3.3: η vs. σ plots for four different volume fractions such that $\phi_5 > \phi_4 > \phi_3 > \phi_2$ in the temperature range of 29°C and 35°C. Similar to ϕ_6, an extra Newtonian plateau can be seen for all ϕs and the overall curves shift downwards with temperature. For ϕ_4 and ϕ_3, weak ST is observed at $T = 32.25$°C and $T = 32$°C respectively and for ϕ_2, ST is observed in the temperature range of 31.5°C and 32.25°C.

Hence, for the FC measurements of the PNIPAM coated particles, we started with Φ_6 and diluted the sample for the consecutive measurements at lower volume fractions. η vs σ plot for ϕ_6 at different temperatures is shown in Figure 3.2 (a). For all temperatures, there appears an extra Newtonian plateau with η in the range of 1 Pa.s to 10 Pa.s, which is normally observed in the suspension of particles in a polymeric liquid and colloidal gels [10, 11]. At lower temperatures where the surface polymers are in the swollen state, the high yield stress arises because of the squeezing of different polymer coatings against each other, which needs to be overcome to produce any flow. It is

followed by the shear thinning behavior with σ, which ends on a second Newtonian plateau. In this region we expect shear-rates to be low enough to cause any noticeable changes in the underlying micro-structures. On further increasing stress, we expect shear-rate to dominate, resulting in rearrangement of the particles into more favorable configuration which causes another decrease in η. With increase in T, second Newtonian plateau broadens and while the high yield stress almost vanishes pointing towards role of polymer brushes for it to be present. At low temperatures prior to the appear-
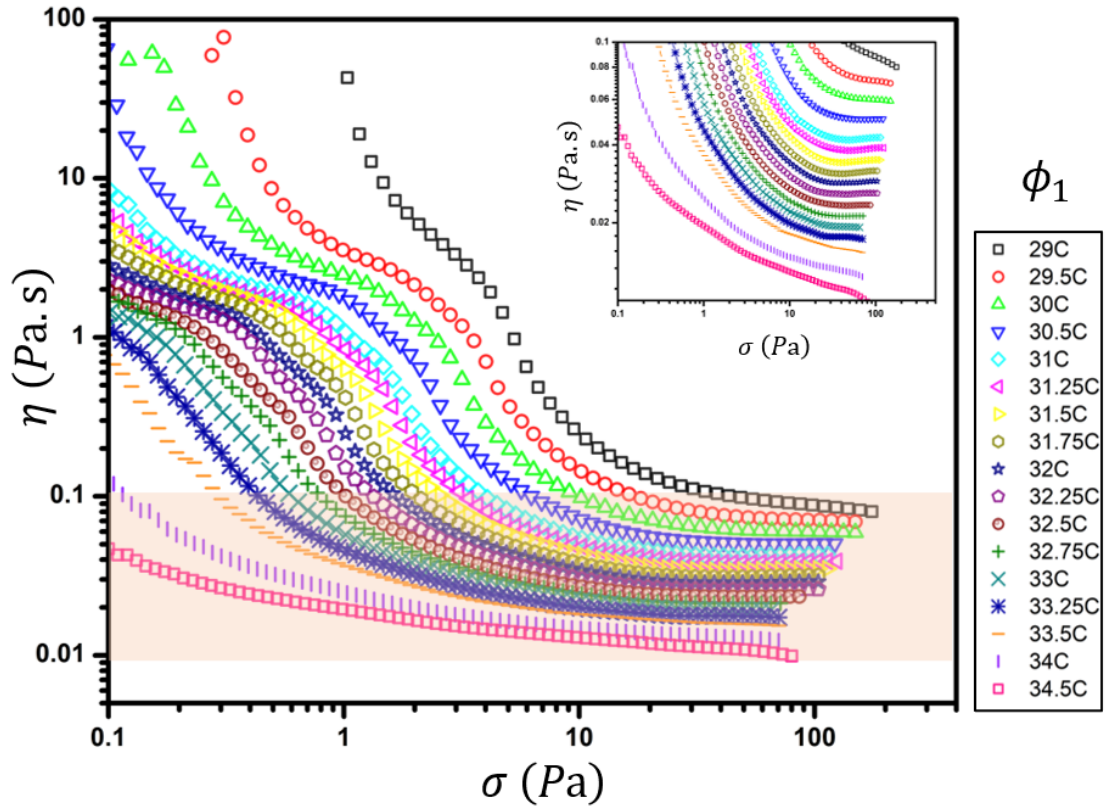
Figure 3.4: FC for ϕ_1 (lowest volume fraction) at different temperatures. For 30.5°C to 32.75° temperature range, ST is observed. Above 32.75°C, suspension transits back from ST to shear thinning. Inset is the zoomed in plot of the shaded region showing clear signatures of ST in intermediate temperature range.

ance of shear thinning, the sample displays high yield stress which decreased as T_{LCST} is approached from below. The decrease in effective volume fraction with T causes the overall curve to shift downwards while the ST exponent β keeps increasing, attaining maximum value at 32°C and stays nearly constant till 33.5°C before starting to become more negative again (Figure 3.2 (b)-(c)). The negative value of β indicates that sus-

pension only behaves like a shear-thinning fluid throughout the temperature range. On diluting the suspension, a similar trend was observed in all flow curves with T (Figure 3.3). Suspension largely behaves like a shear thinning fluid, but weak shear thickening was observed at ϕ_4 and ϕ_3 at $T = 32.5°$ and $32°C$, respectively (Figure 3.3 (b) and (c)). For ϕ_2, ST was observed in a narrow temperature window between $31.5°C$ and $32.25°C$ (Figure 3.3 (d) and 3.5), which broadened further to $30.5°C$ and $32.75°C$ (Figure 3.4 and 3.5) for the most dilute sample ϕ_1. From the prior knowledge, with the decrease
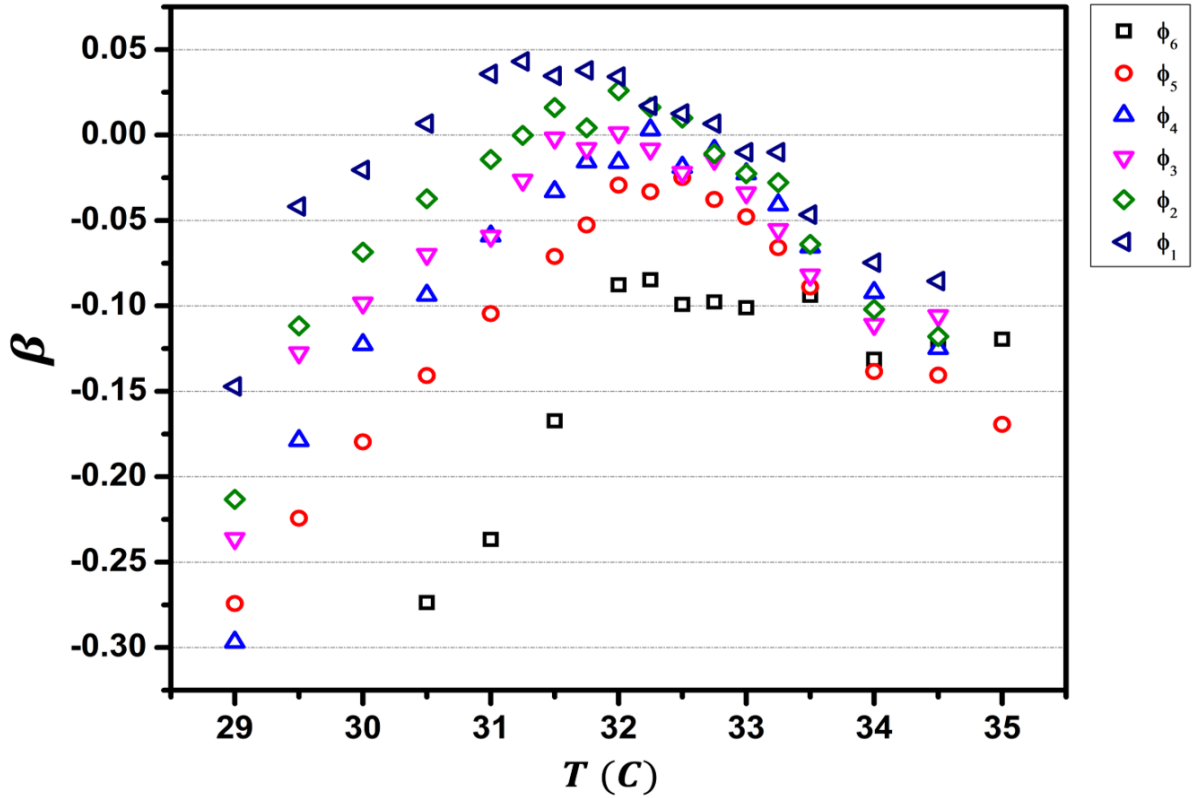
Figure 3.5: β vs. T plots for all ϕs. Volume fractions are in the order: $\phi_6 > \phi_5 > \phi_4 > \phi_3 > \phi_2 > \phi_1$.

in ϕ, suspensions are expected to display a reduction in ST behavior. But in our experiments, even though effective ϕ was decreasing with T, β was found to increase, eventually becoming positive for $\phi \leq \phi_4$. We know that, as T_{LCST} is approached, the collapse of polymer brushes causes the effective aspect ratio α of the rods to increase, which is known to enhance ST behavior [12, 13], we expect only minor changes in α in the temperature window where we observe positive β. Hence we can rule out α as a significant parameter causing ST in our suspension. The only possible parameter

which can account for enhancement of the ST behavior with decrease in effective ϕ with temperature is the surface friction μ [5]. At higher temperatures, the exponent β transits from positive to negative values indicating reemergence of the shear-thinning behavior (Figure 3.5). This is caused by the complete collapse of the PNIPAM brushes above T_{LCST}, resulting in adhesion between the particles due to hydrophobic surface interactions. At higher ϕs (ϕ_6 and ϕ_5), although β increases with temperature, it fails to attain a positive value. One important criteria for the existence of shear thickening window is that, yield stress should comparably be less than the threshold stress required for the frictional network to take over, else yield stress can mask the shear-thickening stress window and no shear thickening is observed in such cases [14]. For $\phi > \phi_4$, it is very likely that this criterion is not fulfilled and causes β to remain less than.

3.1.2 Signature of surface friction enhancement

To solidify our claims that an increase in β with temperature results from the enhancement of μ, we designed an experiment to quantify inter-particle surface interaction at the microscopic level. To do so, 95 μl of a dilute suspension of PNIPAM rods suspended in water were taken in a vial, and 5 μl of 1 mg/ml solution of sodium carboxymethyl cellulose (NaCMC) was added to it. The addition of NaCMC introduces depletion interactions between the surfaces, because of which, when suspension is loaded to a cell, particles settles down and align perfectly along the surface of the cell with time. If the cell is left undisturbed, the rods eventually come in contact with each other to form a dimer-like configuration [15]. Although dimer configuration corresponds to the lowest energy state for the two rods in the presence of a depletion agent, sliding motion between the rods is expected because of the thermal energy $\frac{k_B T}{2}$ per degree of freedom. This kind of sliding motion was clearly observed in our experiments and is shown in Figure 3.6 (a).

To obtain a stable dimer, optical tweezers were used to trap the particles together, and the dynamics of the dimer were captured using a camera at 5 fps at different temperatures starting from 31°C to 34°C. To quantify the sliding motion of the particles in the dimer, particles were individually tracked and identified using ImageJ and Matlab, and all images were transformed to one of the particle's frames of reference. In this new frame of reference, MSD of the second particle given by

$$< r^2(\triangle t) >= \frac{1}{N} \sum_{i=1}^{N} < (r_i(t + \triangle t) - r_i(t))^2 > \tag{3.1}$$
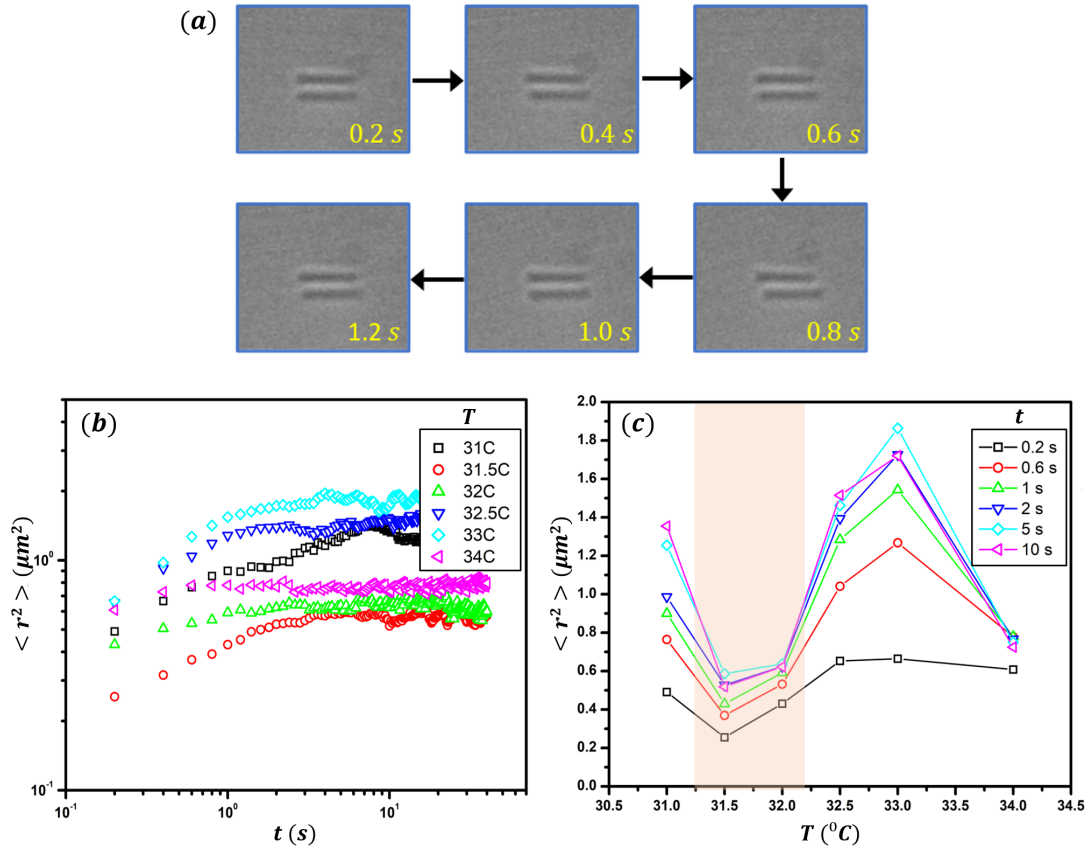
Figure 3.6: (a) Image of a dimer as observed under the microscope at different times. At $t = 0.8$ s, displacement of the lower dimer can clearly be observed. (b) MSD vs time (t) plot of a particle in a frame of reference fixed to the other particle of the dimer at different T. (c) MSD vs Temperature plot at at different times. Decrease in MSD as T is increased from 31°C to 31.5°C indicates lesser sliding motion between the particles which is possible only if μ gets enhanced.

is determined at different temperatures and is shown in Figure 3.6 (b) and (c). At all temperatures, MSD saturates to constant values at longer times, which is expected since the maximum sliding motion of the particles in dimer configuration has an upper bound. With an increase in temperature, one would expect a more rapid and larger sliding motion in the dimer. But in our case, as T is raised from 31°C to 31.5°C, the sliding motion was observed to decrease. MSD at 31.5°C and 32°C is smaller than MSD at 31°C at all times (Figure 3.6 (b) and (c)). Both of these temperatures correspond to a partial collapse of the PNIPAM brushes, with 32°C being the temperature where the maximum value of μ is reported [5]. Hence, slowing down of sliding motion with an increase in temperature is caused by the enhancement of interparticle surface friction,

also explaining the increase in β with temperature in the flow curves. At 34°C, another decrease in the overall value of MSD is observed. One explanation of this transition is 8-10% enhancement of refractive index on raising the temperature 33°C to 34°C, which increases the trapping efficiency of the tweezers [16]. Another possible explanation is the hydrophobic surface interaction between the particles causing them to adhere to each other. Such interactions between the surfaces cause β to decrease again at higher temperatures, as can be seen in Figure 3.5. Hence, our investigation clearly indicates inter-particle surface friction as an important parameter to tune ST in suspensions.

3.2 Flow instabilities in colloidal rods suspension in CST regime

In the DST regime, presence of intermediate region of negative slope in σ vs $\dot{\gamma}$ plot indicate flow instabilities [17, 18]. Such instabilities are not expected in the CST regime since $\dot{\gamma}$ remains a single-valued function for all values of σ. According to the frictional model, ST arises because of the increase in frictional interactions between particles with σ and DST region in the flow curves corresponds to the coexistence of low viscosity Newtonian phase (lubricated interactions) and high viscosity Newtonian phase (frictional interactions). Because of this coexistence, flow instabilities are observed in DST. For anisotropic particles such as colloidal rods, alignment of the rods with respect to each other and the flow direction can change the overall η of the suspension, and unlike isotropic particle suspensions, the temporal variations in the DST regime can have a period of the order of few minutes [19]. Such long variations seem restricted to isotropic particles and are caused by additional rotational degrees of freedom. In our experiments, we have investigated the flow behavior of colloidal rods suspended in a 15:85 water-glycerol mixture in the CST regime.

3.2.1 Suspension behavior under cone-plate confinement

For the cone-plate rheological investigation, a Quartz cone of 25 mm diameter was used along with a steel as a reception plate. We started with $\phi = 0.33$, which already displayed a significant amount of ST. With ϕ, β also increases but stays less than unity, indicating we are still operating in the CST regime (Figure 3.7 (a)). For all ϕs, both forward and reverse curves largely overlap, indicating the absence of both instabilities and irreversibility in the flow behavior. For the highest volume fraction $\phi = 0.40$, one
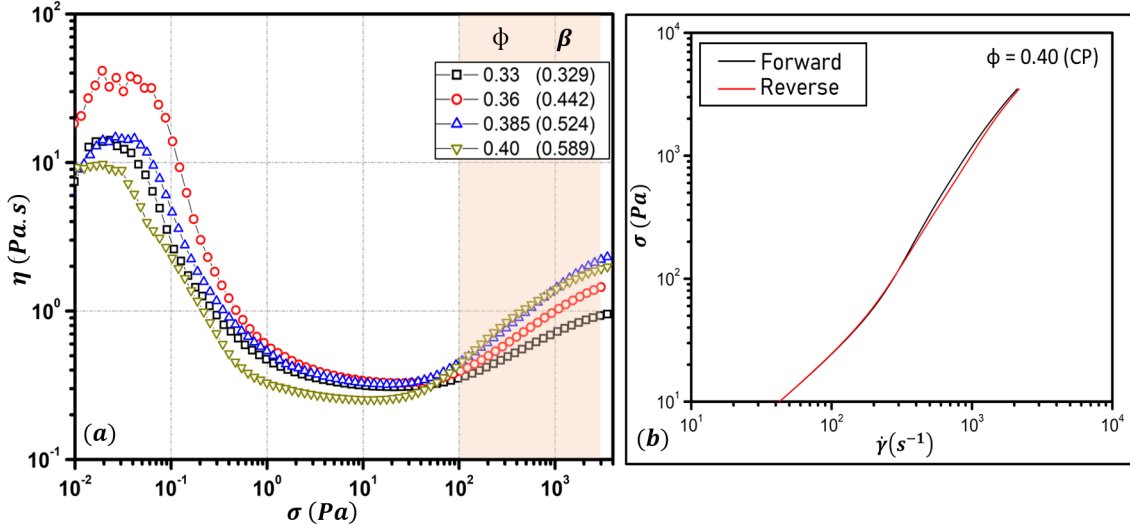
Figure 3.7: (a) Flow curves performed under quartz cone and steel plate confinement of diameter 25 mm. With ϕ, β can be seen increasing as expected. The shaded region corresponds to the stress window in which stress relaxation measurements are performed. (b) Forwards and reverse curve sweeps for $\phi = 0.40$. Both the curves largely overlap indicating absence of any irreversibilities and instabilities.

such forwards and reverse curve is shown in Figure 3.7 (b).

To unravel the presence of any flow instabilities if present, we performed stress relaxation measurements for all ϕs, in the stress window starting from 100 Pa to 3000 Pa (shaded region in Figure 3.7 (a)). For $\phi \leq 0.385$, $\dot{\gamma}$ was found to converge to a fixed value with time for a constant σ. But for $\phi = 0.40$, temporal rich dynamics were observed in a small stress window. Figure 3.8 (a) and (b) displays results from stress relaxation measurements performed at $\phi = 0.385$ and $\phi = 0.40$ respectively and for better comparison, only a small subset of σ values are plotted. For $\phi = 0.40$, oscillations of well defined periodicity were observed above $\sigma = 2500$ Pa. The time period of such oscillations was as large as 300 s ($\sigma = 2625$ Pa), which decayed to zero along with the amplitude of oscillations as σ was increased, vanishing above 2900 Pa. This feature is opposite to what has been observed in DST regime, where oscillation period was found to diverge with σ [19]. To unravel the major underlying contribution to such oscillations, the magnitude of normal force was checked. In CP geometry, the first normal stress difference and the normal force (F_N) have a linear relationship (Equation 2.2).
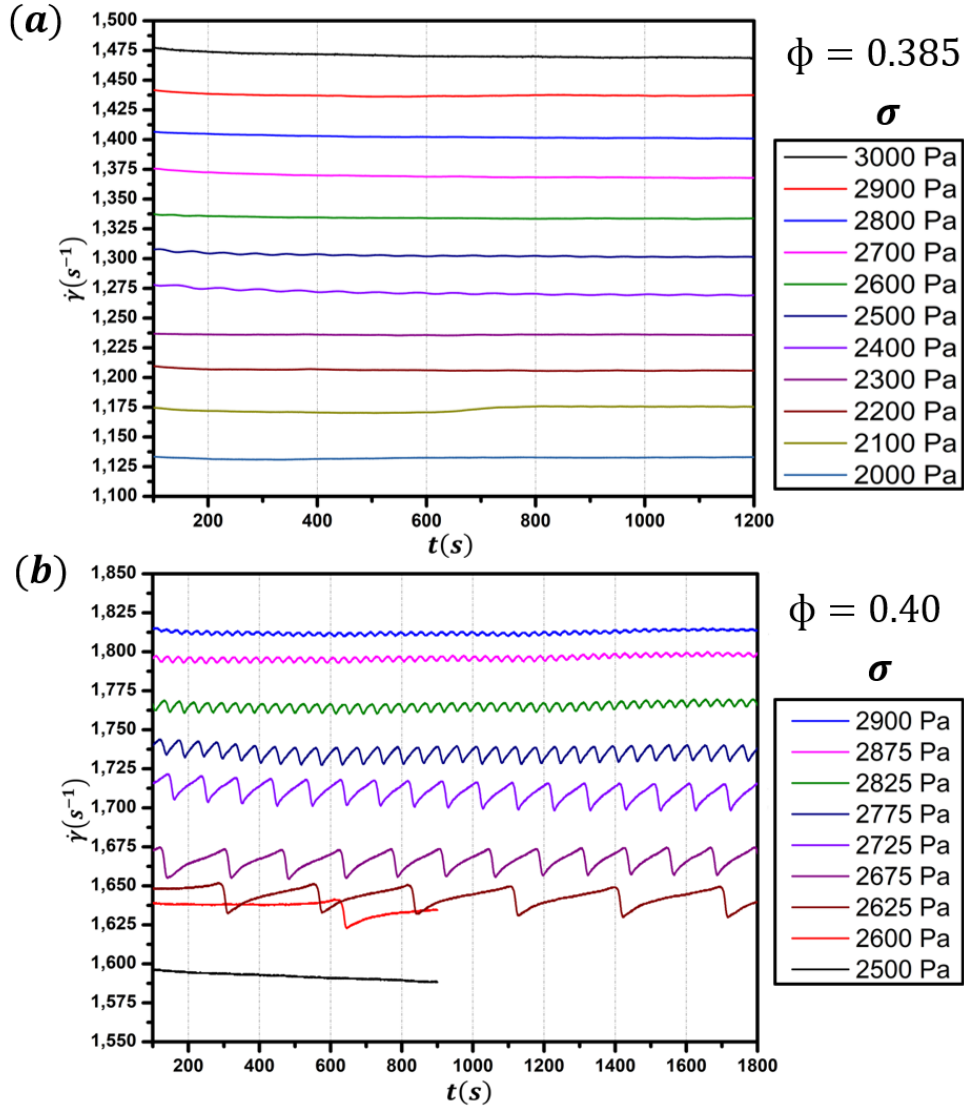
Figure 3.8: (a) and (b) are the stress relaxation curves corresponding to $\phi = 0.385$ and $\phi = 0.4$ respectively. For $\phi = 0.384$, $\dot{\gamma}$ relaxes to a constant values, while instabilities of well defined structure is observed for $\phi = 0.40$.

This allows us to determine the major contribution between the hydrodynamic and the frictional by checking the sign of F_N [20]. Corresponding to all the local minimas in $\dot{\gamma}$, a direct correlation with F_N was observed (Figure 3.9). We found F_N to be -ve at all times in the stress window where the instabilities were observed, and became even more -ve with increase in σ. Corresponding to a decrease in $\dot{\gamma}$ (or increase in η), F_N was also mostly found to abruptly decrease, indicating such oscillations are majorly because of the inter-particle hydrodynamic interactions.
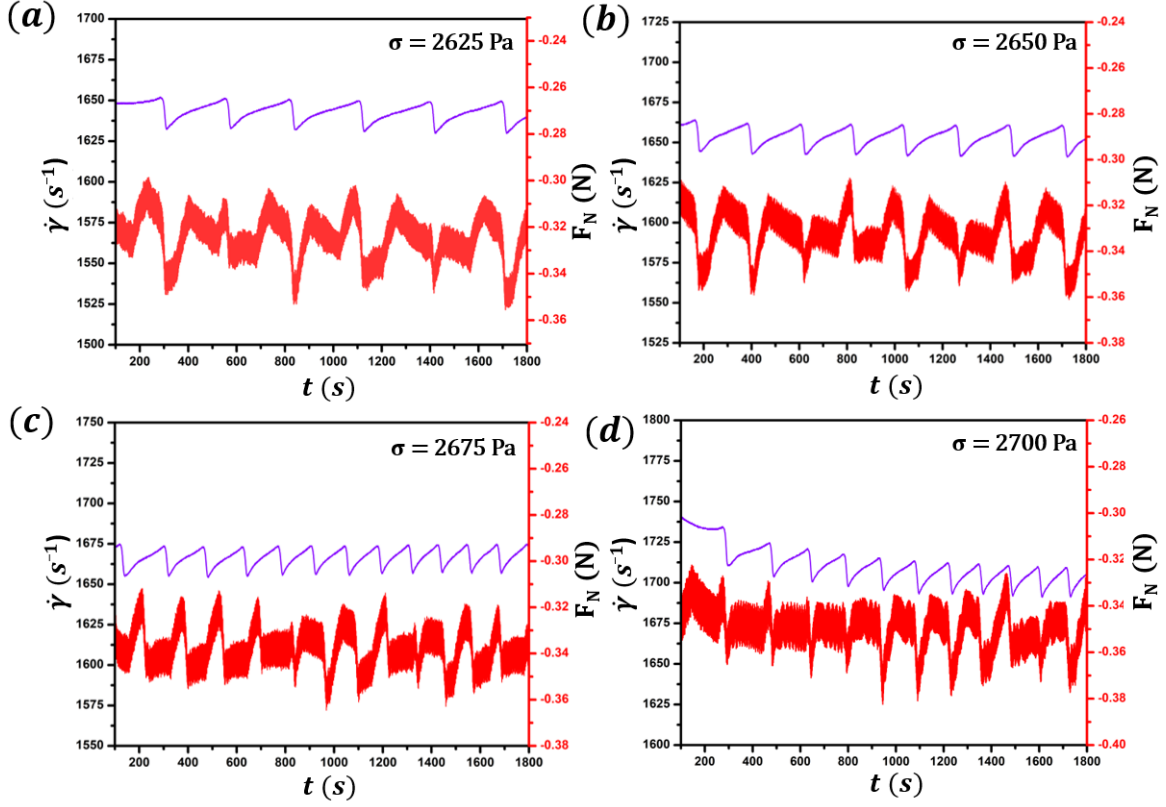
Figure 3.9: (a)-(d) $\dot{\gamma}$ and F_N plot with time for σ = 2625, 2650, 2675 and 2700 Pa respectively. F_N in all plots is always negative pointing towards hydrodynamic interaction as major contribution to oscillations.

3.2.2   Suspension behavior under parallel-plate confinement

For parallel plate rheology, circular steel plates of 25 mm diameter were used. Flow behavior was first studied at 65 μm gap (h), which was further reduced to 35 μm for another set of readings. For all the measurements β was mostly found to increase with ϕ and decrease with confinement (Figure 3.10 (a)-(b)). This phenomenon of decrease in ST with confinement at a given ϕ is well reported and is mainly because of the forced alignment of the rods with increase in confinement, pointing towards the role of particle orientation in shear-thickening [21]. Forwards and reverse sweep measurement for $\phi = 0.385$ and $\phi = 0.40$ largely overlap for both the gaps but slight enhancement in hysteresis is observed for more confined sample (Figure 3.10 (c)-(f)). As the amount of hysteresis is minimal, we again do not expect to observe any flow instabilities. We performed stress relaxation measurement in the CST regime for both the gaps (Figure 3.10), and the results are shown in Figure 3.11.
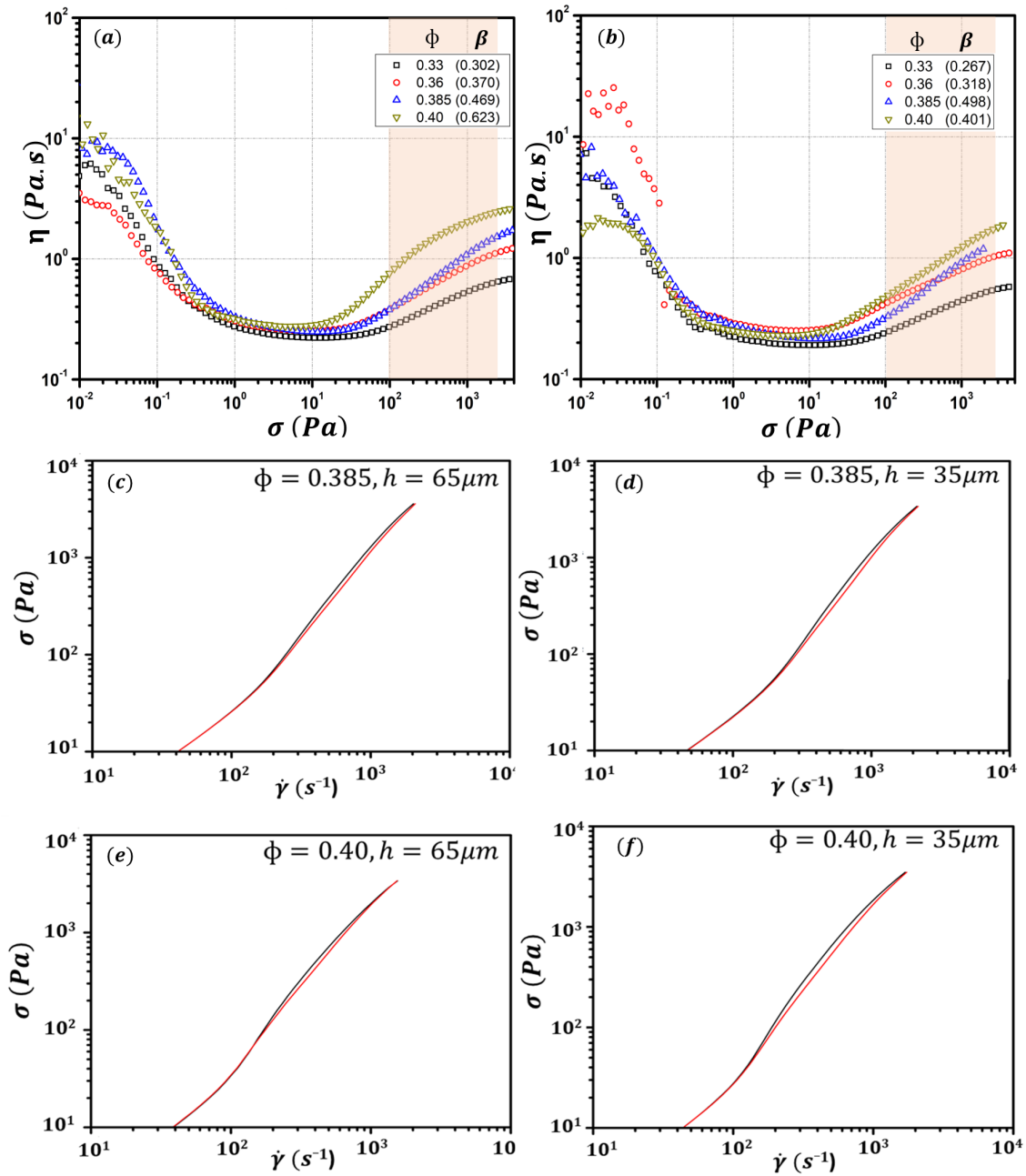
Figure 3.10: (a) and (b) corresponds to flow curves under PP-25 confinement for 65 μm and 35 μm gap respectively. The ϕ and corresponding β are mentioned in the respective plots. Shaded region indicates stress window where stress relaxation measurements were performed.(c)-(f) are forward (red curve) and reverse (black curve) stress sweep plots, corresponding to ϕs and gap size as mentioned in the plots. For all four curves, both red and black curve largely overlap indicating absence of irreversibilities and flow-instabilities.
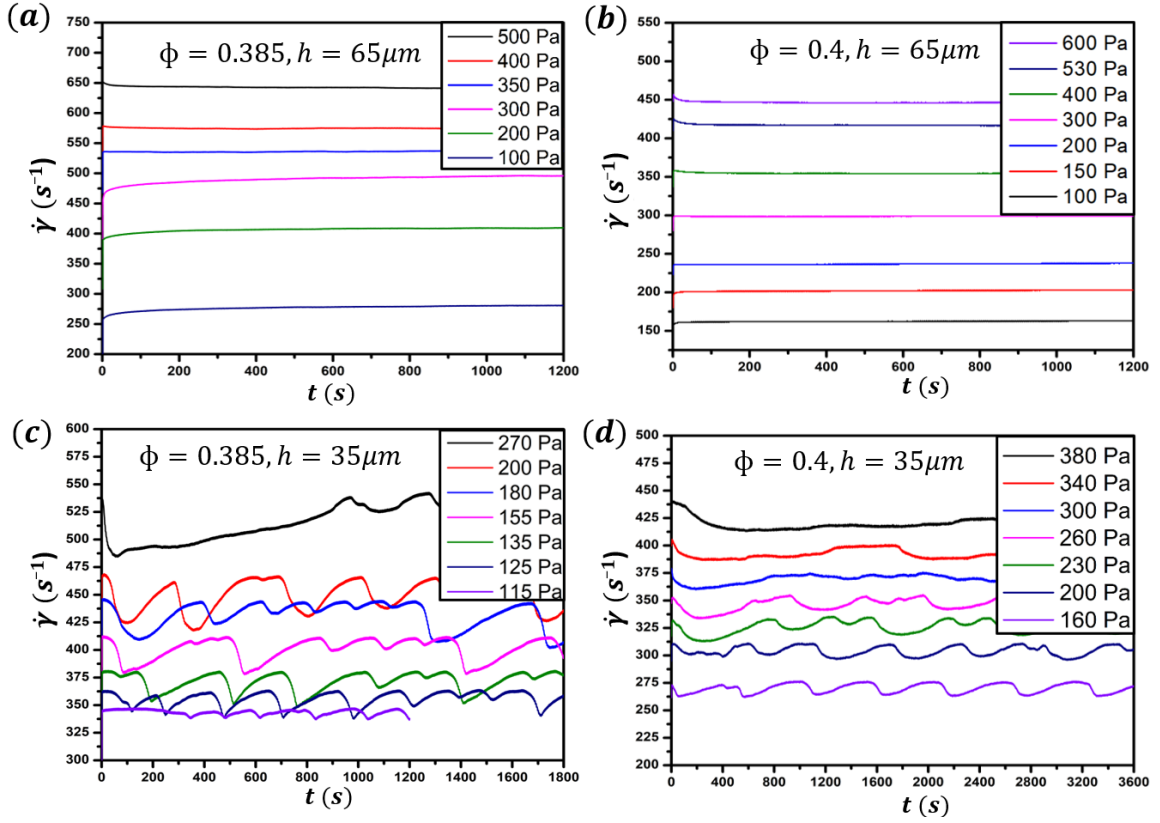
Figure 3.11: (a) and (b) display results from stress relaxation measurements for $\phi = 0.385$ and $\phi = 0.40$ for 65 μm gap. Since $\dot{\gamma}$ converges to a fixed value, flow is stable for this gap. (c)-(d) are stress relaxation measurements corresponding to the same sample show in (a)-(b), when the confinement is increase by lowering the gap to 35 μm.

For $h = 65$ μm, $\dot{\gamma}$ was found to converge to a fixed value with time for all the four ϕs. But on increasing the confinement, rich temporal dynamics were observed, which were previously absent (Figure 3.11 (c)-(d)). For $\phi = 0.33$ and 0.36, no such dynamics were observed at 35 μm gap. The time period of the oscillations for $\phi=0.385$ and $\phi=0.40$ was observed to be approximately 200 s and 400 s respectively, and was found to diverge as σ is increased. Oscillations observed in this case are very distinct as they seem not to have a very well-defined period. Since instabilities were triggered only when the confinement was increased, we can conclude that such instabilities are not only a function of ϕ but also depends on the confinement as a parameter. As of now, we do know that increase in η at a constant σ can only occur when the rods disorient from the direction of flow, causing more streamline deviation. Still, such oscillation also requires cooperative misalignment of the rods to produce any noticeable change in bulk η. Above that, having such periodic variations in $\dot{\gamma}$ also indicates the systematic

nature of cooperative misalignment, which still needs more investigation.

Hence, from our experiments with suspension of colloidal rods, we have for the first time showed that flow instabilities which were expected to exist only in DST regime, can also exist in the CST regime. The origin of such fluctuations is purely hydrodynamic as indicated by normal force measurements and can be triggered either by increasing the ϕ or by increasing the confinement.

Bibliography

[1] Matthieu Wyart and Micheal E Cates. Discontinuous shear thickening without inertia in dense non-brownian suspensions. *Physical review letters*, 112(9):098302, 2014.

[2] Ryohei Seto, Romain Mari, Jeffrey F Morris, and Morton M Denn. Discontinuous shear thickening of frictional hard-sphere suspensions. *Physical review letters*, 111(21):218301, 2013.

[3] Jeffrey F Morris. Lubricated-to-frictional shear thickening scenario in dense suspensions. *Physical Review Fluids*, 3(11):110508, 2018.

[4] Gaurasundar M Conley, Sofi Nöjd, Marco Braibanti, Peter Schurtenberger, and Frank Scheffold. Superresolution microscopy of the volume phase transition of pnipam microgels. *Colloids and Surfaces A: Physicochemical and Engineering Aspects*, 499:18–23, 2016.

[5] Yunlong Yu, Bernard D Kieviet, Fei Liu, Igor Siretanu, Edit Kutnyánszky, G Julius Vancso, and Sissi de Beer. Stretching of collapsed polymers causes an enhanced dissipative response of pnipam brushes near their lcst. *Soft Matter*, 11(43):8508–8516, 2015.

[6] Debby P Chang, John E Dolbow, and Stefan Zauscher. Switchable friction of stimulus-responsive hydrogels. *Langmuir*, 23(1):250–257, 2007.

[7] Anke Kuijk, Alfons Van Blaaderen, and Arnout Imhof. Synthesis of monodisperse, rodlike silica colloids with tunable aspect ratio. *Journal of the American Chemical Society*, 133(8):2346–2349, 2011.

[8] Jia Guo, Wuli Yang, Changchun Wang, Jia He, and Jiyao Chen. Poly (n-isopropylacrylamide)-coated luminescent/magnetic silica microspheres: preparation, characterization, and biomedical applications. *Chemistry of Materials*, 18(23):5554–5562, 2006.

[9] Zhimin Xing, Congling Wang, Jie Yan, Li Zhang, Lan Li, and Liusheng Zha. Dual stimuli responsive hollow nanogels with ipn structure for temperature controlling drug loading and ph triggering drug release. *Soft Matter*, 7(18):7992–7997, 2011.

[10] AJ Poslinski, ME Ryan, RK Gupta, SG Seshadri, and FJ Frechette. Rheological behavior of filled polymeric systems i. yield stress and shear-thinning effects. *Journal of Rheology*, 32(7):703–735, 1988.

[11] N Koumakis, P Ballesta, R Besseling, WCK Poon, JF Brady, and G Petekidis. Colloidal gels under shear: Strain rate effects. In *AIP Conference Proceedings*, volume 1518, pages 365–371. American Institute of Physics, 2013.

[12] Yilan Ye, Han Xiao, Kelley Reaves, Billy McCulloch, Jared F Mike, and Jodie L Lutkenhaus. Effect of nanorod aspect ratio on shear thickening electrolytes for safety-enhanced batteries. *ACS Applied Nano Materials*, 1(6):2774–2784, 2018.

[13] Nicole M James, Huayue Xue, Medha Goyal, and Heinrich M Jaeger. Controlling shear jamming in dense suspensions via the particle aspect ratio. *Soft matter*, 15(18):3649–3654, 2019.

[14] Eric Brown, Nicole A Forman, Carlos S Orellana, Hanjun Zhang, Benjamin W Maynor, Douglas E Betts, Joseph M DeSimone, and Heinrich M Jaeger. Generality of shear thickening in dense suspensions. *Nature materials*, 9(3):220–224, 2010.

[15] W Li and HR Ma. Depletion interactions between two spherocylinders. *The European Physical Journal E*, 16(2):225–231, 2005.

[16] Brett W Garner, Tong Cai, Santaneel Ghosh, Zhibing Hu, and Arup Neogi. Refractive index change due to volume-phase transition in polyacrylamide gel nanospheres for optoelectronics and bio-photonics. *Applied physics express*, 2(5):057001, 2009.

[17] Zhongcheng Pan, Henri de Cagny, Bart Weber, and Daniel Bonn. S-shaped flow curves of shear thickening suspensions: Direct observation of frictional rheology. *Physical Review E*, 92(3):032202, 2015.

[18] Michiel Hermes, Ben M Guy, Wilson CK Poon, Guilhem Poy, Michael E Cates, and Matthieu Wyart. Unsteady flow and particle migration in dense, non-brownian suspensions. *Journal of Rheology*, 60(5):905–916, 2016.

[19] Vikram Rathee, Srishti Arora, Daniel L Blair, Jeffrey S Urbach, AK Sood, and Rajesh Ganapathy. Role of particle orientational order during shear thickening in suspensions of colloidal rods. *Physical Review E*, 101(4):040601, 2020.

[20] John R Royer, Daniel L Blair, and Steven D Hudson. Rheological signature of frictional interactions in shear thickening suspensions. *Physical review letters*, 116(18):188301, 2016.

[21] Eric Brown, Hanjun Zhang, Nicole A Forman, Benjamin W Maynor, Douglas E Betts, Joseph M DeSimone, and Heinrich M Jaeger. Shear thickening in densely

packed suspensions of spheres and rods confined to few layers. *Journal of Rheology*, 54(5):1023–1046, 2010.

Chapter 4

Conclusion

Understanding mechanisms giving rise to different types of non-Newtonian behavior in dense suspension has been of great interest to researchers for the past many decades. With the advancement in sophisticated techniques, such as high resolution fast confocal methods, in situ scattering methods, and more versatile rheometers, it has become possible to study the underlying structures and behavior of such fluids in great detail. For small shear stress values, experiments have pointed out towards rearrangement of particles into layers, resulting in lesser dissipation due to decrease in inter-particle collisions, causing the suspension to shear thin [1, 2]. These results are backed by fast confocal microscopy experiments, which indicated the presence of periodic dense regions along the gradient direction [3]. At higher stresses, shear-thickening behavior is observed. In this region, in situ imaging becomes tricky because of the higher shear rates and is only possible at volume fractions close to DST, where shear rates are still under experimental limitations. Few such experiments have confirmed the formation of hydroclusters in the ST region [3], verifying the hydrodynamic theory of ST, but fails to give any insight of transition from CST to DST.

An alternate theory called the inter-particle friction-based theory (Wyart and Cates model) explained both CST and DST as a transition of interactions between particles from lubricated to frictional and paved the way for all-new strategies to tune ST in suspensions [4]. Inspired by the frictional-based model, we adopted an approach to tune ST in the suspension of colloidal silica rods by grafting stimulus-responsive polymer called PNIPAM on the surface of the particles. PNIPAM undergoes coil-globular transition when the lower critical solvent temperature (LCST) is approached from below [5, 6, 7, 8]. This transition causes effective volume occupied by the particles to decrease while enhancing overall surface friction, which is maximum just below LCST. A similar picture is depicted by our temperature ramp experiment results, in which η

decreases by approximately seven orders of magnitude on raising the temperature from 25°C to 34°C. In the temperature controlled flow curve measurements, β increases with temperature, only to become negative above T_{LCST} where the surface of the particles adhere due to hydrophobic interactions. Enhancement in surface roughness was investigated by analyzing the sliding motion of two rods past each other while confining them in dimer configuration using depletion interaction and optical tweezers. With temperature, enhanced sliding motion is expected in principle due to increase in thermal energy, but we observed a slowing down of the dynamics with a minor raise of 0.5°C in temperature. Another decrease in sliding motion at 34°C was observed, which is either caused by enhancement of refractive index [9] or due to adhesion between particles, verifying non-monotonic behavior of β at higher temperatures. The collective picture that emerges from our experiments points out towards inter-particle friction as an essential variable to tune ST in suspensions of anisotropic particles such as rods. Further fine-tuning of ST behavior can be performed by either changing the pH of the solvent and by fine-tuning the thickness of the polymer coating. The initial choice of suspended particle shape to be coated with PNIPAM may also enhance or diminish the ST behavior of the final suspension with temperature.

Previous investigations on dense suspension of colloidal rods near DST confirmed flow instabilities because of the strong coupling between particle orientations and the flow, and underestimation of the shear thickening exponent with ϕ as predicted by Wyart and Cates model [10]. To better understand the ST mechanism in suspensions of anisotropic particles, it is essential to understand different contributions to ST in such systems. These contributions include hydrodynamic clustering, surface to surface inter-particle frictional interactions, and particle orientation with respect to the flow direction. Through our experiments with colloidal rods suspended in a glycerol-water mixture, we have tried to unravel flow instabilities in the CST regime. The presence of such instabilities can be considered a good confirmation of particle orientation contribution to ST. Our experiments were carried out under three different confinements: cone-plate confinement with a diameter of 25 mm, parallel-plate confinement with a diameter of 25 mm, and gap size of 0.065mm and 0.035 mm respectively. Stress sweeps and stress relaxation measurements were carried in all three configurations for $\phi = 0.33$, 0.36, 0.385, and 0.40. Under CP confinement, β is a monotonic increasing function of ϕ and is always less than unity signifying the CST regime. No temporal dynamics in $\dot{\gamma}$ or η were observed until $\phi = 0.40$, where well-defined periodic oscillations of the time period as large as 300 s were observed. The presence of instabilities with increasing ϕ points out that even in CST, rotational degree of freedom of the particles starts contributing to ST. The origin of such oscillations was dominatingly hydrodynamic

as normal force (F_N) was always less than zero in all stress relaxation measurements. Under parallel-plate confinement, β was again always less than unity. No such instabilities were observed for the 0.065 mm gap for all values of ϕs. In contrast, for the 0.035 mm gap, clear variations in $\dot{\gamma}$ were detected for $\phi = 0.385$ and 0.40. Although one expects rods alignment to be even greater when the gap size is reduced, such a restrictive environment seems to trigger cooperative misalignment of rods resulting in such well-defined and structured variation in bulk viscosity. For all the FCs in all three geometries, even though instabilities were clearly observed, reverse and forward stress sweep curves were largely overlapping, with slight enhancement in hysteresis when the gap size was reduced in PP. This minor presence of hysteresis points towards the reversible nature of the FCs and, unlike in the DST regime, fails to predict the presence of flow instabilities. Hence our experiments with colloidal rod suspension unraveled the presence of flow instabilities in a very narrow stress window in the CST regime, which were previously expected to exist only during DST, and also pointed out that such instabilities are a function of ϕ as well as confinement. Dynamics of cooperative misalignment of the rods to display periodic variations in η over time still need more investigation and can be taken as future scope of work.

Bibliography

[1] RL Hoffman. Discontinuous and dilatant viscosity behavior in concentrated suspensions. i. observation of a flow instability. *Transactions of the Society of Rheology*, 16(1):155–173, 1972.

[2] RL Hoffman. Discontinuous and dilatant viscosity behavior in concentrated suspensions. ii. theory and experimental tests. *Journal of Colloid and Interface Science*, 46(3):491–506, 1974.

[3] Xiang Cheng, Jonathan H McCoy, Jacob N Israelachvili, and Itai Cohen. Imaging the microscopic structure of shear thinning and thickening colloidal suspensions. *Science*, 333(6047):1276–1279, 2011.

[4] Matthieu Wyart and ME Cates. Discontinuous shear thickening without inertia in dense non-brownian suspensions. *Physical review letters*, 112(9):098302, 2014.

[5] Niklas Nordgren and Mark W Rutland. Tunable nanolubrication between dual-responsive polyionic grafts. *Nano letters*, 9(8):2984–2990, 2009.

[6] Debby P Chang, John E Dolbow, and Stefan Zauscher. Switchable friction of stimulus-responsive hydrogels. *Langmuir*, 23(1):250–257, 2007.

[7] Yang Wu, Meirong Cai, Xiaowei Pei, Yongmin Liang, and Feng Zhou. Switching friction with thermal-responsive gels. *Macromolecular rapid communications*, 34(22):1785–1790, 2013.

[8] Yunlong Yu, Bernard D Kieviet, Fei Liu, Igor Siretanu, Edit Kutnyánszky, G Julius Vancso, and Sissi de Beer. Stretching of collapsed polymers causes an enhanced dissipative response of pnipam brushes near their lcst. *Soft Matter*, 11(43):8508–8516, 2015.

[9] Brett W Garner, Tong Cai, Santaneel Ghosh, Zhibing Hu, and Arup Neogi. Refractive index change due to volume-phase transition in polyacrylamide gel nanospheres for optoelectronics and bio-photonics. *Applied physics express*, 2(5):057001, 2009.

[10] Vikram Rathee, Srishti Arora, Daniel L Blair, Jeffrey S Urbach, AK Sood, and Rajesh Ganapathy. Role of particle orientational order during shear thickening in suspensions of colloidal rods. *Physical Review E*, 101(4):040601, 2020.